

SPECIALIZATION PROJECT IN THEORETICAL PHYSICS

Supercurrent transport by Andreev Bound States in external field

Author:

Anna Ursula Birkeland BRØYN

Supervisor

Prof. Jacob Linder

December 17, 2016



NTNU – Trondheim
Norwegian University of
Science and Technology

Abstract

Here you give a summary of your work and your results. This is like a management summary and should be written in a clear and easy language, without many difficult terms and without abbreviations. Everything you present here must be treated in more detail in the main report. You should not give any references to the report in the summary – just explain what you have done and what you have found out. The Summary and Conclusions should be no more than two pages.

You may assume that you have got three minutes to present to the Rector of NTNU what you have done and what you have found out as part of your thesis. (He is an intelligent person, but does not know much about your field of expertise.)

Acknowledgement

I would like to thank the following persons for their great help during ...

If the project has been carried out in cooperation with an external partner (e.g., a company), you should acknowledge the contribution and give thanks to the involved persons.

You should also acknowledge the contributions made by your supervisor(s).

O.N.

(Your initials)

Contents

Abstract	i
Acknowledgement	ii
Contents	iii
Abbreviations	v
1 Introduction	1
2 Superconductivity	3
2.1 The Meissner effect	3
2.2 BCS theory	4
2.2.1 The BCS Hamiltonian	4
2.2.2 Mean field Approximation	5
2.2.3 Diagonalization of the BCS Hamiltonian	6
2.2.4 Bogoliubov-de Gennes Equations	8
2.3 Andreev reflection	9
2.4 Josephson current	10
2.5 Free Energy	12
3 Physical System	13
4 Andreev Bound State energies in SNS-junction	15
4.1 ABS energies without barriers or applied field	15
4.1.1 Andreev reflection amplitude	15
4.1.2 Bohr-Sommerfeld quantization	16
4.1.3 ABS energy	17
4.2 ABS energies with barriers	17
4.2.1 Boundary conditions	18

4.2.2	Wave functions in the superconduction region	18
4.2.3	Wave functions in the normal region	20
4.2.4	ABS energy	21
4.3	ABS energies with applied field	22
4.3.1	Guage transformation	22
4.3.2	Bohr-Sommerfeld quantization condition	23
4.3.3	ABS energy	24
5	Andreev Bound State Current in SNS-junction	25
5.1	ABS current without barriers or applied field	26
5.2	ABS current with barriers	26
5.3	ABS current with applied field	27
5.3.1	Uniform magnetic field	28
5.3.2	Sinusoidal field varying along the junction	31
5.3.3	Sinusoidal field varying along the interfaces	36
6	Conclusion and outlook	43
A	Additional Information	45
A.1	Commutation relations	45
A.2	The pauli matrices	45
Bibliography		46

Abbreviations

FTA Fault tree analysis

MTTF Mean time to failure

RAMS Reliability, availability, maintainability, and safety

Chapter 1

Introduction

In 1911, H. K. Onnes discovered that the electrical resistance in mercury vanished when it was cooled down to a temperature of 4.2 K [1]. This was the first observation of superconductivity and it would go two more decades before W. Meissner and R. Ochsenfeld, in 1933, discovered a second fundamental property of superconductivity, namely the expulsion of magnetic fields below a certain threshold value [2]. The absence of electrical resistance and the expulsion of the magnetic field are macroscopic quantum mechanical effects of which a microscopical description was missing for another two decades. This was finally presented by Bardeen, Cooper and Schieffer in 1957, now known as the BCS theory [3]. The theory propose that the supercurrent in a superconductor is transported via pairs of electrons, known as *Cooper pairs*, which condense into an electronic superfluid in which the Cooper pairs can travel without resistance.

When a superconductor (S) is placed in contact with a normal metal (N), Cooper pairs will leak from the superconductor and into the normal metal. This effect is known as the *proximity effect* [4], and allow for superconducting-like properties in materials which originally were non-superconducting. As the Meissner effect expels magnetic fields, superconductivity and magnetism rarely coexists in bulk materials. However, when hybrid structures are exposed to magnetic fields, the proximity effect allows for interplay between superconductivity and magnetism, giving rise to a variety of interesting effects. In recent years new techniques have allowed resolving properties on smaller length scales and lower temperatures, and this has renewed the interest of the subject [5]. There is now a good understanding of many electronic and transport properties of hybrid SN structures, but there are still many unexplored aspects of the dependency the magnetic field has on those properties.

In 1963 Rowell [6] observed that a superconductor-insulator-superconductor, exposed to a magnetic field, would have critical current that oscillates in a certain manner, known as Fraunhofer

oscillations. It is understood that these oscillations are a consequence of circulating current vortices appearing in the insulator between the superconductors, due to quantum interference. The vortices are known as Josephson vortices and have later been observed in several SNS-junctions [7, 8], as well as junctions with other materials such as graphene [9–12] and topological insulators [13–16].

In wide junctions ($W \gg L$) research has shown that the vortices are arranged in a chain along the superconducting interface [17–21]. It is well-known that this pattern is modified by the insulating barriers if $W \approx L$ [22–24], and in newer research it was found that if the Fermi surface is warped, the vortices are modified into two-dimensional vortex lattice [25]. In any cases the critical current decays as Fraunhofer oscillations when the field strength is increased, although the decay rate under certain conditions has varied [25, 26]. To our knowledge there has not been any research on the effect a *modulated* magnetic field has on these, and the object of this thesis is to understand how we can control the vortex pattern and critical current using modulated magnetic fields.

The outline of the thesis is as follows. In chapter 2 we will give the necessary background theory, including an explanation of the Meissner effect and BCS theory, as well as supercurrent transport theory in hybrid structures. In chapter 3 we define the physical system to consider, namely a two-dimensional SNS-junction which will be subject to external magnetic fields. In chapter 4 we consider two methods, with different advantages, for deriving the energy levels of the system. These energy levels will in chapter 5 be used to find the current in the junction. In chapter 6 we summarize the results in a conclusion followed by an outlook for future work.

Chapter 2

Superconductivity

Two fundamental properties associated to superconductivity are 1) zero electrical resistance giving rise to *supercurrents*, for temperatures below some critical temperature T_c and 2) complete expulsion of magnetic field below T_c , known as the Meissner effect [2, 27]. The theory behind these properties was presented by Bardeen, Cooper and Schrieffer in 1957 and is known as the BCS-theory [3].

2.1 The Meissner effect

Meissner and Ochsenfeld discovered in 1933 [2] that applied magnetic field, H , below some critical limit H_c , would be expelled in the superconductor for temperatures below T_c , resulting in zero field inside the superconductor, $B = \mu_0(H+M) = 0$, so that $M = -H$. The superconductor is thus a perfect diamagnet with susceptibility

$$\chi = \frac{dM}{dH} = -1. \quad (2.1)$$

This is called the Meissner effect and is a consequence of induced screening supercurrents at the surface of the superconductor. No current can exist only on the surface of a material as this would imply a finite current in a layer of zero thickness requiring infinite density of free charge. Consequently, the screening current must exist at some finite distance, λ_L , into the superconductor and thus letting the external magnetic field penetrate to a depth λ_L . This penetration depth will depend on the density of superconducting carriers (Cooper pairs) and is a result from the London equations [28] and Ampere's law.

The Meissner effect breaks down as the external field is increased to above the critical limit H_c . Depending on the material we will then get full (in type I superconductors) or partial (in

type II superconductors) penetration of magnetic flux and the superconductor will go from the superconducting state into the normal or mixed state, respectively.

2.2 BCS theory

The BCS theory is based on the appearance of so called *Cooper pairs* which conventionally are formed by a phonon-mediated attractive interaction between two electrons overwinning the Coulomb repulsion [3]. The Cooper pairs are bosonic...

2.2.1 The BCS Hamiltonian

The Hamiltonian of the system will consist of two parts, describing the non-interacting and interacting electrons, respectively. A given state is defined by the momentum \mathbf{k} and spin σ . In the second quantization formalism the annihilation- and creation operators, $c_{\mathbf{k},\sigma}$ and $c_{\mathbf{k},\sigma}^\dagger$, will destroy and create an electron in the corresponding state, respectively. The number operator $n_{\mathbf{k},\sigma} = c_{\mathbf{k},\sigma}^\dagger c_{\mathbf{k},\sigma}$ counts the number of electrons in the state. The non-interacting part of the Hamiltonian will simply be the energy of each state, $\epsilon_{\mathbf{k}} = \hbar^2 k^2 / 2m$, times the number operator and summed over all states. This will thus be the first term in Hamiltonian (2.2). The interacting part of the Hamiltonian will describe a scattering process where two electrons into the states (\mathbf{k}, σ) and (\mathbf{k}', σ') are scattered to the states $(\mathbf{k} + \mathbf{q}, \sigma)$ and $(\mathbf{k}' - \mathbf{q}, \sigma')$, i.e. (\mathbf{k}, σ) and $(\mathbf{k} + \mathbf{q}, \sigma)$ are destroyed by the annihilation operators while $(\mathbf{k}' - \mathbf{q}, \sigma')$ and (\mathbf{k}', σ') are created by the creation operators. We must also include a matrix element $V_{\mathbf{k},\mathbf{k}'}$ including both the attractive phonon-mediated interaction and the repulsive Coulomb interaction, between the electrons. The second term in the Hamiltonian (2.2) describe this interaction. The total Hamiltonian including both the non-interacting and the interacting term is thus given as

$$H = \sum_{\mathbf{k},\sigma} \epsilon_{\mathbf{k}} c_{\mathbf{k},\sigma}^\dagger c_{\mathbf{k},\sigma} + \sum_{\mathbf{k},\mathbf{k}',\mathbf{q},\sigma,\sigma'} V_{\mathbf{k},\mathbf{k}'}(\mathbf{q}, \omega) c_{\mathbf{k}+\mathbf{q},\sigma}^\dagger c_{\mathbf{k}'-\mathbf{q},\sigma'}^\dagger c_{\mathbf{k},\sigma} c_{\mathbf{k}',\sigma'}. \quad (2.2)$$

We define $\epsilon_{\mathbf{k}} \equiv \epsilon_{\mathbf{k}} - \mu$ as the energy above the Fermi surface. We have used the chemical potential, μ , in the place of the Fermi energy, ϵ_F , as these two quantities are essentially the same in all relevant cases. The attractive interaction will only be valid in a small energy range, ω , above the Fermi-surface, and for electrons on opposite sides of the Fermi-surface. We may therefore let $\mathbf{k}' = -\mathbf{k}$. Due to the Pauli principle we will in most cases find the electrons in the Cooper pairs in opposite spin states, so we will also let $\sigma' = -\sigma$. By now changing the dummy indices, the

Hamiltonian takes the form

$$H - \mu N = \sum_{\mathbf{k}, \sigma} \varepsilon_{\mathbf{k}} c_{\mathbf{k}, \sigma}^\dagger c_{\mathbf{k}, \sigma} + \sum_{\mathbf{k}, \mathbf{k}'} V_{\mathbf{k}, \mathbf{k}'} c_{\mathbf{k}, \uparrow}^\dagger c_{-\mathbf{k}, \downarrow}^\dagger c_{\mathbf{k}', \uparrow} c_{-\mathbf{k}', \downarrow}, \quad (2.3)$$

where N is the number of electrons. Henceforth we will write H in place of $H - \mu N$.

2.2.2 Mean field Approximation

We will use mean field approximation to simplify the Hamiltonian and assume the fluctuations around the expectation values to be small such that we can write

$$c_{-\mathbf{k}, \downarrow} c_{\mathbf{k}, \uparrow} = \langle c_{-\mathbf{k}, \downarrow} c_{\mathbf{k}, \uparrow} \rangle + c_{-\mathbf{k}, \downarrow} c_{\mathbf{k}, \uparrow} - \langle c_{-\mathbf{k}, \downarrow} c_{\mathbf{k}, \uparrow} \rangle \equiv \langle c_{-\mathbf{k}, \downarrow} c_{\mathbf{k}, \uparrow} \rangle + \delta_{\mathbf{k}}, \quad (2.4)$$

and only keep δ to the first order. By also defining the *gap parameter* as follows

$$\Delta_{\mathbf{k}'} = \sum_{\mathbf{k}} V_{\mathbf{k}, \mathbf{k}'} \langle c_{-\mathbf{k}, \downarrow} c_{\mathbf{k}, \uparrow} \rangle, \quad (2.5)$$

the Hamiltonian will simplify to

$$\begin{aligned} H &= \sum_{\mathbf{k}, \sigma} \varepsilon_{\mathbf{k}} c_{\mathbf{k}, \sigma}^\dagger c_{\mathbf{k}, \sigma} + \sum_{\mathbf{k}} \left[\Delta_{\mathbf{k}}^* c_{\mathbf{k}, \uparrow} c_{-\mathbf{k}, \downarrow} + \Delta_{\mathbf{k}} c_{\mathbf{k}, \uparrow}^\dagger c_{-\mathbf{k}, \downarrow}^\dagger - \Delta_{\mathbf{k}} \langle c_{\mathbf{k}, \uparrow}^\dagger c_{-\mathbf{k}, \downarrow}^\dagger \rangle \right] \\ &= - \sum_{\mathbf{k}} \Delta_{\mathbf{k}} \langle c_{\mathbf{k}, \uparrow}^\dagger c_{-\mathbf{k}, \downarrow}^\dagger \rangle + \sum_{\mathbf{k}} \varepsilon_{\mathbf{k}} \left[c_{\mathbf{k}, \uparrow}^\dagger c_{\mathbf{k}, \uparrow} + c_{-\mathbf{k}, \downarrow}^\dagger c_{-\mathbf{k}, \downarrow} \right] + \sum_{\mathbf{k}} \left[\Delta_{\mathbf{k}}^* c_{\mathbf{k}, \uparrow} c_{-\mathbf{k}, \downarrow} + \Delta_{\mathbf{k}} c_{\mathbf{k}, \uparrow}^\dagger c_{-\mathbf{k}, \downarrow}^\dagger \right] \\ &= \sum_{\mathbf{k}} \left[\varepsilon_{\mathbf{k}} - \Delta_{\mathbf{k}} \langle c_{\mathbf{k}, \uparrow}^\dagger c_{-\mathbf{k}, \downarrow}^\dagger \rangle \right] + \sum_{\mathbf{k}} \varepsilon_{\mathbf{k}} \left[c_{\mathbf{k}, \uparrow}^\dagger c_{\mathbf{k}, \uparrow} - c_{-\mathbf{k}, \downarrow}^\dagger c_{-\mathbf{k}, \downarrow} \right] + \sum_{\mathbf{k}} \left[\Delta_{\mathbf{k}}^* c_{\mathbf{k}, \uparrow} c_{-\mathbf{k}, \downarrow} + \Delta_{\mathbf{k}} c_{\mathbf{k}, \uparrow}^\dagger c_{-\mathbf{k}, \downarrow}^\dagger \right] \quad (2.6) \\ &= E_0 + \sum_{\mathbf{k}} \begin{pmatrix} c_{\mathbf{k}, \uparrow}^\dagger & c_{-\mathbf{k}, \downarrow} \end{pmatrix} \begin{pmatrix} \varepsilon_{\mathbf{k}} & \Delta_{\mathbf{k}} \\ \Delta_{\mathbf{k}}^* & -\varepsilon_{\mathbf{k}} \end{pmatrix} \begin{pmatrix} c_{\mathbf{k}, \uparrow} \\ c_{-\mathbf{k}, \downarrow}^\dagger \end{pmatrix} \equiv E_0 + \sum_{\mathbf{k}} \varphi'_{\mathbf{k}} H'_{\mathbf{k}} \varphi'_{\mathbf{k}} \end{aligned}$$

where we have used the standard commutation relations for fermions (A.1c) and defined

$$E_0 \equiv \sum_{\mathbf{k}} \left[\varepsilon_{\mathbf{k}} - \Delta_{\mathbf{k}} \langle c_{\mathbf{k}, \uparrow}^\dagger c_{-\mathbf{k}, \downarrow}^\dagger \rangle \right], \quad H'_{\mathbf{k}} = \begin{pmatrix} \varepsilon_{\mathbf{k}} & \Delta_{\mathbf{k}} \\ \Delta_{\mathbf{k}}^* & -\varepsilon_{\mathbf{k}} \end{pmatrix} \quad \text{and} \quad \varphi'_{\mathbf{k}} \equiv \begin{pmatrix} c_{\mathbf{k}, \uparrow} \\ c_{-\mathbf{k}, \downarrow}^\dagger \end{pmatrix}.$$

The Hamiltonian (2.6) can be diagonalized by inserting $U_{\mathbf{k}} U_{\mathbf{k}}^\dagger = I$, where U is a unitary matrix:

$$U_{\mathbf{k}} = \begin{pmatrix} u_{\mathbf{k}} & -v_{\mathbf{k}}^* \\ v_{\mathbf{k}} & u_{\mathbf{k}}^* \end{pmatrix}, \quad U_{\mathbf{k}}^\dagger = \begin{pmatrix} u_{\mathbf{k}}^* & v_{\mathbf{k}}^* \\ -v_{\mathbf{k}} & u_{\mathbf{k}} \end{pmatrix} \quad (2.7)$$

and $u_{\mathbf{k}}$ and $v_{\mathbf{k}}$ satisfy the relation

$$|u_{\mathbf{k}}|^2 + |v_{\mathbf{k}}|^2 = 1. \quad (2.8)$$

This will be satisfied if we write $u_{\mathbf{k}}$ and $v_{\mathbf{k}}$ on the form

$$u_{\mathbf{k}} = e^{i\alpha} \cos \theta_{\mathbf{k}}, \quad v_{\mathbf{k}} = e^{i\beta} \sin \theta_{\mathbf{k}}. \quad (2.9)$$

Our Hamiltonian will now be on the form

$$H = E_0 + \sum_{\mathbf{k}} \varphi_{\mathbf{k}}^\dagger H_{\mathbf{k}} \varphi_{\mathbf{k}} \quad (2.10)$$

with $H_{\mathbf{k}} = U_{\mathbf{k}}^\dagger H'_{\mathbf{k}} U_{\mathbf{k}}$ and $\varphi_{\mathbf{k}} \equiv U_{\mathbf{k}}^\dagger \varphi'_{\mathbf{k}}$, i.e.

$$\varphi_{\mathbf{k}} \equiv \begin{pmatrix} \gamma_{\mathbf{k},\uparrow} \\ \gamma_{-\mathbf{k},\downarrow}^\dagger \end{pmatrix} = \begin{pmatrix} u_{\mathbf{k}}^* & v_{\mathbf{k}}^* \\ -v_{\mathbf{k}} & u_{\mathbf{k}} \end{pmatrix} \begin{pmatrix} c_{\mathbf{k},\uparrow} \\ c_{-\mathbf{k},\downarrow}^\dagger \end{pmatrix}. \quad (2.11)$$

The new fermionic operators $\gamma_{\mathbf{k},\uparrow}$ and $\gamma_{-\mathbf{k},\downarrow}^\dagger$ are describing excitations of so called *quasiparticles*.

2.2.3 Diagonalization of the BCS Hamiltonian

We need to find what values of $u_{\mathbf{k}}$ and $v_{\mathbf{k}}$ that will satisfy the relation (2.8) and diagonalize $H_{\mathbf{k}}$:

$$\begin{aligned} H_{\mathbf{k}} &= U_{\mathbf{k}}^\dagger H'_{\mathbf{k}} U_{\mathbf{k}} = \begin{pmatrix} u_{\mathbf{k}}^* & v_{\mathbf{k}}^* \\ -v_{\mathbf{k}} & u_{\mathbf{k}} \end{pmatrix} \begin{pmatrix} \varepsilon_{\mathbf{k}} & \Delta_{\mathbf{k}} \\ \Delta_{\mathbf{k}}^* & -\varepsilon_{\mathbf{k}} \end{pmatrix} \begin{pmatrix} u_{\mathbf{k}} & -v_{\mathbf{k}}^* \\ v_{\mathbf{k}} & u_{\mathbf{k}}^* \end{pmatrix} \\ &= \begin{pmatrix} \varepsilon_{\mathbf{k}}(|u_{\mathbf{k}}|^2 - |v_{\mathbf{k}}|^2) + \Delta_{\mathbf{k}} u_{\mathbf{k}}^* v_{\mathbf{k}} + \Delta_{\mathbf{k}}^* u_{\mathbf{k}} v_{\mathbf{k}}^* & \Delta_{\mathbf{k}} u_{\mathbf{k}}^{*2} - \Delta_{\mathbf{k}}^* v_{\mathbf{k}}^{*2} - 2\varepsilon_{\mathbf{k}} u_{\mathbf{k}}^* v_{\mathbf{k}}^* \\ \Delta_{\mathbf{k}}^* u_{\mathbf{k}}^2 - \Delta_{\mathbf{k}} v_{\mathbf{k}}^2 - 2\varepsilon_{\mathbf{k}} u_{\mathbf{k}} v_{\mathbf{k}} & -[\varepsilon_{\mathbf{k}}(|u_{\mathbf{k}}|^2 - |v_{\mathbf{k}}|^2) + \Delta_{\mathbf{k}} u_{\mathbf{k}}^* v_{\mathbf{k}} + \Delta_{\mathbf{k}}^* u_{\mathbf{k}} v_{\mathbf{k}}^*] \end{pmatrix}. \end{aligned} \quad (2.12)$$

For the off-diagonal elements to be zero we must have $\Delta_{\mathbf{k}}^* u_{\mathbf{k}}^2 - \Delta_{\mathbf{k}} v_{\mathbf{k}}^2 - 2\varepsilon_{\mathbf{k}} u_{\mathbf{k}} v_{\mathbf{k}} = 0$. We write $u_{\mathbf{k}}$ and $v_{\mathbf{k}}$ on the form given in equation (2.9) and write $\Delta_{\mathbf{k}} = |\Delta_{\mathbf{k}}| e^{i\varphi}$. This yields

$$\begin{aligned} 0 &= \Delta_{\mathbf{k}}^* u_{\mathbf{k}}^2 - \Delta_{\mathbf{k}} v_{\mathbf{k}}^2 - 2\varepsilon_{\mathbf{k}} u_{\mathbf{k}} v_{\mathbf{k}} \\ &= |\Delta_{\mathbf{k}}| e^{i(\alpha+\beta)} \cos^2 \theta \left(e^{i(\alpha-\beta-\varphi)} - e^{-i(\alpha-\beta-\varphi)} \tan^2 \theta_{\mathbf{k}} - 2 \frac{\varepsilon_{\mathbf{k}}}{|\Delta_{\mathbf{k}}|} \tan \theta_{\mathbf{k}} \right), \end{aligned}$$

which gives

$$\alpha - \beta = \varphi \quad \text{and} \quad \tan \theta_{\mathbf{k}} = -\frac{\varepsilon_{\mathbf{k}}}{|\Delta_{\mathbf{k}}|} \pm \sqrt{\frac{\varepsilon_{\mathbf{k}}^2}{|\Delta_{\mathbf{k}}|^2} + 1}. \quad (2.13)$$

$u_{\mathbf{k}}$ and $v_{\mathbf{k}}$ will thus be satisfied by

$$\begin{aligned} |u_{\mathbf{k}}|^2 &= \cos^2 \theta = \frac{1}{2} \left(1 \pm \frac{\varepsilon_{\mathbf{k}}^{\pm}}{\sqrt{\varepsilon_{\mathbf{k}}^{\pm 2} + |\Delta_{\mathbf{k}}|^2}} \right) \\ |v_{\mathbf{k}}|^2 &= \sin^2 \theta = \frac{1}{2} \left(1 \mp \frac{\varepsilon_{\mathbf{k}}^{\pm}}{\sqrt{\varepsilon_{\mathbf{k}}^{\pm 2} + |\Delta_{\mathbf{k}}|^2}} \right). \end{aligned} \quad (2.14)$$

We let $\varepsilon_{\mathbf{k}}^+ > 0$ and $\varepsilon_{\mathbf{k}}^- < 0$ and notice that we get $|u_{\mathbf{k}}| = 1$ and $|v_{\mathbf{k}}| = 0$ when $\Delta_{\mathbf{k}} = 0$, i.e. when there is no attraction between the electrons and thus in the limit of the *normal* state, according to equation (2.5). We calculate the diagonal terms of $H_{\mathbf{k}}$ (2.12) and find

$$H_{\mathbf{k}} = \begin{pmatrix} E_{\mathbf{k}} & 0 \\ 0 & -E_{\mathbf{k}} \end{pmatrix} \quad (2.15)$$

where we have defined

$$E_{\mathbf{k}} = \sqrt{\varepsilon_{\mathbf{k}}^2 + |\Delta_{\mathbf{k}}|^2}. \quad (2.16)$$

as the quasiparticle excitation energy. It is now clear why $\Delta_{\mathbf{k}}$ is referred to as the *gap-parameter* as it gives a gap in the excitation spectrum of the quasiparticles $\varphi_{\mathbf{k}}$. Moreover, we get

$$k^{\pm} = k_F \sqrt{1 + \frac{\varepsilon_{\mathbf{k}}^{\pm}}{\mu}} = k_F \sqrt{1 \pm \frac{\sqrt{E_{\mathbf{k}}^2 - |\Delta_{\mathbf{k}}|^2}}{\mu}} \quad (2.17)$$

where $\mu = \hbar^2 k_F / 2m$ and $\varepsilon_{\mathbf{k}}^{\pm} = \pm \sqrt{E_{\mathbf{k}} - |\Delta_{\mathbf{k}}|^2}$ is obtained from equation (2.16). We notice how we get a fourfold degeneracy of relevant states, $(k^+, k^-, -k^+, -k^-)$, for each $E_{\mathbf{k}}$. From equation (2.14) we see that the quasiparticle excitation $\gamma_{\mathbf{k},\uparrow}^{\dagger}$ from equation (2.11) will be electronlike, since we have $u_{\mathbf{k}} \rightarrow 1$ and $v_{\mathbf{k}} \rightarrow 0$ as $\Delta \rightarrow 0$ and $c_{\mathbf{k},\uparrow}^{\dagger}$ creates an electron while $c_{-\mathbf{k},\downarrow}$ destroys an electron, leaving a hole. Similarly, $\gamma_{\mathbf{k},\uparrow}$ will be holelike. Moreover, from equation (2.17) we see that $\pm k^+$ ($\pm k^-$) corresponds to energy above(below) the Fermi surface and thus $\pm k^+$ ($\pm k^-$) are electron(hole)-like excitations.

For convenience we introduce a new variable, η , defined in the following way

$$\eta = \begin{cases} \arccos\left(\frac{E_{\mathbf{k}}}{|\Delta_{\mathbf{k}}|}\right), & \text{if } E_{\mathbf{k}} < |\Delta_{\mathbf{k}}| \\ i \operatorname{arccosh}\left(\frac{E_{\mathbf{k}}}{|\Delta_{\mathbf{k}}|}\right), & \text{if } E_{\mathbf{k}} > |\Delta_{\mathbf{k}}|. \end{cases} \quad (2.18)$$

Then we can write

$$\frac{|u_{\mathbf{k}}|}{|\nu_{\mathbf{k}}|} = e^{i\eta}. \quad (2.19)$$

2.2.4 Bogoliubov-de Gennes Equations

In the description above we assumed the Hamiltonian to be position-invariant so that the wave functions could be considered as simple plane waves, $\sim \exp(i\mathbf{k} \cdot \mathbf{r})$. We took the potential $V(\mathbf{r})$ and the vector potential, \mathbf{A} , to be zero and the simply replaced the Hamiltonian for a single particle system,

$$h(\mathbf{r}) = \frac{1}{2m} \left(\frac{\hbar}{i} \nabla - q\mathbf{A} \right)^2 - \mu(\mathbf{r}) + V(\mathbf{r}), \quad (2.20)$$

with $\varepsilon_{\mathbf{k}} = \hbar^2 k^2 / 2m - \mu$. For systems where we can not do this simplification we introduce field operators:

$$\psi(\mathbf{r}, t) \equiv \sum_{\mathbf{k}} U(\mathbf{r}, t) \varphi_{\mathbf{k}}, \quad \psi^\dagger(\mathbf{r}, t) \equiv \sum_{\mathbf{k}} \varphi_{\mathbf{k}}^\dagger U^\dagger(\mathbf{r}, t) \quad (2.21)$$

and rewrite the Hamiltonian in equation (2.6) as

$$H = E_0 + \int d^3 r \psi^\dagger(\mathbf{r}, t) \begin{pmatrix} h(\mathbf{r}) & \Delta(\mathbf{r}) \\ \Delta^*(\mathbf{r}) & -h(\mathbf{r}) \end{pmatrix} \psi(\mathbf{r}, t) \equiv E_0 + \int d^3 r \psi^\dagger(\mathbf{r}, t) H(\mathbf{r}) \psi(\mathbf{r}, t). \quad (2.22)$$

Again the Hamiltonian may be diagonalized by setting $U^\dagger(\mathbf{r}, t) H(\mathbf{r}) U(\mathbf{r}, t) = H_{\mathbf{k}}$, or equally $H(\mathbf{r}) U(\mathbf{r}, t) = U(\mathbf{r}, t) H_{\mathbf{k}}$, where $H_{\mathbf{k}}$ is on the form given in equation (2.15). By separating these equations for each eigenvalue in $H_{\mathbf{k}}$ we get the *Bogoliubov de Gennes equations* (BdG equations) [29]:

$$\begin{aligned} \begin{pmatrix} h(\mathbf{r}) & \Delta(\mathbf{r}) \\ \Delta^*(\mathbf{r}) & -h(\mathbf{r}) \end{pmatrix} \begin{pmatrix} u(\mathbf{r}, t) \\ v(\mathbf{r}, t) \end{pmatrix} &= E_{\mathbf{k}} \begin{pmatrix} u(\mathbf{r}, t) \\ v(\mathbf{r}, t) \end{pmatrix}, \\ \begin{pmatrix} -h(\mathbf{r}) & -\Delta^*(\mathbf{r}) \\ -\Delta(\mathbf{r}) & h(\mathbf{r}) \end{pmatrix} \begin{pmatrix} -v(\mathbf{r}, t) \\ u(\mathbf{r}, t) \end{pmatrix} &= E_{\mathbf{k}} \begin{pmatrix} -v(\mathbf{r}, t) \\ u(\mathbf{r}, t) \end{pmatrix}. \end{aligned} \quad (2.23)$$

From equation (2.11) we have $\gamma_{\mathbf{k},\uparrow}^\dagger = u(\mathbf{r}, t) c_{\mathbf{k},\uparrow}^\dagger + v(\mathbf{r}, t) c_{-\mathbf{k},\downarrow}$. By writing $\gamma_{\mathbf{k},\sigma}^\dagger = u_\sigma(\mathbf{r}, t) c_{\mathbf{k},\sigma}^\dagger + v_{-\sigma}(\mathbf{r}, t) c_{-\mathbf{k},-\sigma}$ and $\gamma_{\mathbf{k},\sigma} = u_\sigma(\mathbf{r}, t) c_{-\mathbf{k},-\sigma}^\dagger + v_{-\sigma}(\mathbf{r}, t) c_{\mathbf{k},\sigma}$, we can represent $\gamma_{\mathbf{k},\sigma}^\dagger$ and $\gamma_{\mathbf{k},\sigma}$ by the vectors $\Psi_{e,\sigma}$ and

$\Psi_{h,\sigma}$, respectively, where Ψ is a vector of the form $(u_\uparrow, u_\downarrow, v_\uparrow, v_\downarrow)^T$. We get:

$$\begin{aligned} \gamma_{\mathbf{k},\uparrow}^\dagger \rightarrow \Psi_{e,\uparrow} &= \begin{pmatrix} u(\mathbf{r}, t) \\ 0 \\ 0 \\ v(\mathbf{r}, t) \end{pmatrix}, & \gamma_{-\mathbf{k},\downarrow}^\dagger \rightarrow \Psi_{e,\downarrow} &= \begin{pmatrix} 0 \\ u(\mathbf{r}, t) \\ -v(\mathbf{r}, t) \\ 0 \end{pmatrix}, \\ \gamma_{\mathbf{k},\uparrow} \rightarrow \Psi_{h,\uparrow} &= \begin{pmatrix} v^*(\mathbf{r}, t) \\ 0 \\ 0 \\ u^*(\mathbf{r}, t) \end{pmatrix}, & \gamma_{-\mathbf{k},\downarrow} \rightarrow \Psi_{h,\downarrow} &= \begin{pmatrix} 0 \\ -v^*(\mathbf{r}, t) \\ u^*(\mathbf{r}, t) \\ 0 \end{pmatrix}. \end{aligned} \quad (2.24)$$

We define the 2×2 -matrices $\hat{H}(\mathbf{r}) \equiv \hat{\sigma}_0 h(\mathbf{r})$ and $\hat{\Delta}(\mathbf{r}) \equiv i\hat{\sigma}_2 \Delta(\mathbf{r})$ where $\hat{\sigma}_0$ is the identity matrix and $\hat{\sigma}_i$ with ($i = 1, 2, 3$) are the Pauli matrices, see equation (A.2) in the appendix. Moreover, we define $\vec{u}(\mathbf{r}, t) \equiv (u_\uparrow(\mathbf{r}, t) \ u_\downarrow(\mathbf{r}, t))^T$ and $\vec{v}(\mathbf{r}, t) \equiv (v_\uparrow(\mathbf{r}, t) \ v_\downarrow(\mathbf{r}, t))^T$. The BdG-equations (2.23) can then be written more compact:

$$\begin{pmatrix} \hat{H}(\mathbf{r}) & \hat{\Delta}(\mathbf{r}) \\ \hat{\Delta}^\dagger(\mathbf{r}) & -\hat{H}(\mathbf{r}) \end{pmatrix} \begin{pmatrix} \vec{u}(\mathbf{r}, t) \\ \vec{v}(\mathbf{r}, t) \end{pmatrix} = E_{\mathbf{k}} \begin{pmatrix} \vec{u}(\mathbf{r}, t) \\ \vec{v}(\mathbf{r}, t) \end{pmatrix}. \quad (2.25)$$

2.3 Andreev reflection

When an electron with momentum, $\mathbf{k}^+ = k_x^+ \hat{x} + k_y^+ \hat{y} + k_z^+ \hat{z}$, and spin, σ , in the normal metal is propagating towards the interface between the normal metal and a superconductor, it will be scattered with certain probabilities of transmission and reflection. We choose the coordinate system such that the intersection is placed in the yz -plane, see figure !!!REFFIG!!!. There are two possible ways the electron could be transmitted and reflected. The electron may be transmitted into the superconductor as an electron-like quasiparticle such that the energy of the transmitted quasiparticle is on the *same* side of the Fermi surface, i.e. with momentum $\mathbf{q}^+ = q_x^+ \hat{x} + q_y^+ \hat{y} + q_z^+ \hat{z}$ and spin σ , or as a hole-like quasiparticle by crossing the Fermi surface, i.e. with momentum $\mathbf{q}^- = -q_x^- \hat{x} + q_y^- \hat{y} + q_z^- \hat{z}$ and spin σ . The x -component have negative sign since the wave direction of a hole is opposite of the direction of its wave vector, as explained in section 2.2.3 !!!OBS PASS PÅ AT DETTE ER FORKLART RETT STED!!!. The electron may be reflected, either in the normal way, i.e. as an electron with momentum, $\mathbf{k}_r^+ = -k_x^+ \hat{x} + k_y^+ \hat{y} + k_z^+ \hat{z}$, and the same spin, σ , or by *Andreev reflection* [30]. In Andreev reflection the incoming electron goes into the superconductor and form a Cooper pair with an electron of opposite spin, leaving a reflected hole with momentum $\mathbf{k}^- = k_x^- \hat{x} + k_y^- \hat{y} + k_z^- \hat{z}$ and spin $-\sigma$. We will in this section ignore the spin de-

generacy and express the wave vectors as $\psi(\mathbf{r}) = (u_{\mathbf{k}}(\mathbf{r}) \ v_{\mathbf{k}}(\mathbf{r}))^T$. In the simplest case we consider plane waves, i.e. energies, $E_{\mathbf{k}}$, as given in equation (2.16) with corresponding wave numbers, \mathbf{k}^\pm and wave vectors of the form [31]

$$\psi_{k^+}(\mathbf{r}) = \begin{pmatrix} u_0 e^{i\alpha} \\ v_0 e^{i\beta} \end{pmatrix} e^{i\mathbf{k}^+ \cdot \mathbf{r}} \quad \text{and} \quad \psi_{k^-}(\mathbf{r}) = \begin{pmatrix} v_0 e^{-i\beta} \\ u_0 e^{-i\alpha} \end{pmatrix} e^{i\mathbf{k}^- \cdot \mathbf{r}}, \quad (2.26)$$

in correspondance with equation (2.24). The incoming, reflected and transmitted wave vectors will in this notation take the form

$$\begin{aligned} \psi_i(\mathbf{r}) &= \begin{pmatrix} 1 \\ 0 \end{pmatrix} e^{i\mathbf{k}^+ \cdot \mathbf{r}} \\ \psi_r(\mathbf{r}) &= r_{ee} \begin{pmatrix} 1 \\ 0 \end{pmatrix} e^{i\mathbf{k}_r^+ \cdot \mathbf{r}} + r_{eh} \begin{pmatrix} 0 \\ 1 \end{pmatrix} e^{i\mathbf{k}^- \cdot \mathbf{r}} \\ \psi_t(\mathbf{r}) &= t_{ee} \begin{pmatrix} u_0 e^{i\alpha} \\ v_0 e^{i\beta} \end{pmatrix} e^{i\mathbf{q}^+ \cdot \mathbf{r}} + t_{eh} \begin{pmatrix} v_0 e^{-i\beta} \\ u_0 e^{-i\alpha} \end{pmatrix} e^{i\mathbf{q}^- \cdot \mathbf{r}}, \end{aligned} \quad (2.27)$$

where r_{ee} , r_{eh} , t_{ee} , and t_{eh} represent the probabilities of normal reflection, Andreev reflection, electron-like transmission and hole-like transmission, respectively. We notice how the normal reflection will give opposite value of the x -component of the wave vector while the others remain the same. In the Andreev reflection, however, we have retro reflection and the hole will thus move along the same path as the incoming electron. See figure !!!!FIGREF!!!!.

In equation (2.16) we found that only energies above the energy gap, $|\Delta_{\mathbf{k}}|$, are allowed for the quasiparticles. Consequently, when $E_{\mathbf{k}} < |\Delta_{\mathbf{k}}|$ the amplitudes t_{ee} and t_{eh} will be zero and only reflection (either normal or Andreev reflection) is allowed. If there is no barrier at the interface, there will be no normal reflection and only Andreev reflection will be allowed. States with such energies in SNS-junctions would thus be trapped in the normal metal by the Andreev reflections and are referred to as Andreev Bound States (ABS).

2.4 Josephson current

A Josephson junction is a device consisting of two superconductors that is brought into contact via a *weak link*, in which the *critical current* is much lower. The critical current is the maximum supercurrent that can exist in the superconductor and is related to the density of Cooper pairs. Josephson effect describes two important phenomena of supercurrents in a Josephson junction [32]. Firstly Josephson predicted that supercurrents would flow through the Josephson junction

even without any applied voltage. Secondly if the junction was driven by an external current exceeding the critical current, electromagnetic waves would be radiated. We will here focus on the first phenomena.

There are several ways to construct a weak link, and we will in this project consider the *SNS-junction*, i.e. a junction consisting of two superconductors, separated by a normal metal.

The Josephson current is in general dependent on the full quasiparticle spectrum, but in the short junction regime the continuous spectrum ($E > \Delta$) does not contribute to the current.
blblbabla

The number operator, N , of the Cooper pairs in the superconductor, and the superconducting phase φ are canonical conjugate variables. Hence

$$\dot{N} = -\frac{1}{\hbar} \frac{\partial H}{\partial \varphi} \quad \dot{\varphi} = \frac{1}{\hbar} \frac{\partial H}{\partial N}. \quad (2.28)$$

The tunnelig current from a superconductor S_1 with number of particles N_1 to a superconductor S_2 with number of particles N_2 through a weak link will be given as

$$I = q \dot{N}_1 = -q \dot{N}_2 \quad (2.29)$$

where $q = -2e$ is the charge of a Cooper pair. Using equation (2.28) in this expression gives

$$I = \frac{2e}{\hbar} \frac{\partial H}{\partial \varphi_1} = -\frac{2e}{\hbar} \frac{\partial H}{\partial \varphi_2}. \quad (2.30)$$

The phase difference is defined $\Delta\varphi = \varphi_1 - \varphi_2$, and as only the phase difference, not the individual phases, has physical meaning, we let $\partial\varphi_1 \rightarrow \partial\Delta\varphi$ and $\partial\varphi_2 \rightarrow -\partial\Delta\varphi$. Hence

$$I = \frac{2e}{\hbar} \frac{\partial H}{\partial(\Delta\varphi)}. \quad (2.31)$$

Taking the expectation value of this gives

$$I = \frac{2e}{\hbar} \frac{\partial F}{\partial(\Delta\varphi)} \quad (2.32)$$

where F is the free energy, since

$$\frac{\partial F}{\partial(\Delta\varphi)} = -\frac{1}{\beta} \frac{1}{Z} \frac{\partial Z}{\partial(\Delta\varphi)} = -\frac{1}{\beta Z} \text{Tr} \left[-\beta \frac{\partial H}{\partial(\Delta\varphi)} e^{-\beta H} \right] = \frac{1}{Z} \text{Tr} \left[\frac{\partial H}{\partial(\Delta\varphi)} e^{-\beta H} \right] = \left\langle \frac{\partial H}{\partial(\Delta\varphi)} \right\rangle \quad (2.33)$$

with Z as the partition function:

$$Z = e^{-\beta F} = \text{Tr} \left[e^{-\beta H} \right]. \quad (2.34)$$

This shows how the current is *phase-driven*. blablabla

2.5 Free Energy

The diagonal Hamiltonian in equation (2.10) is on the form as a free fermion gas:

$$\begin{aligned} H &= E_0 + \sum_{\mathbf{k}} \begin{pmatrix} \gamma_{\mathbf{k},\uparrow}^\dagger & \gamma_{-\mathbf{k},\downarrow} \end{pmatrix} \begin{pmatrix} E_{\mathbf{k}} & 0 \\ 0 & -E_{\mathbf{k}} \end{pmatrix} \begin{pmatrix} \gamma_{\mathbf{k},\uparrow} \\ \gamma_{-\mathbf{k},\downarrow}^\dagger \end{pmatrix} \\ &= E_0 + \sum_{\mathbf{k}} \left[E_{\mathbf{k}} \gamma_{\mathbf{k},\uparrow}^\dagger \gamma_{\mathbf{k},\uparrow} - E_{\mathbf{k}} \left(1 - \gamma_{-\mathbf{k},\downarrow}^\dagger \gamma_{-\mathbf{k},\downarrow} \right) \right] \\ &= E_0 + \sum_{\mathbf{k}} E_{\mathbf{k}} (N_{\uparrow} + N_{\downarrow} - 1) \end{aligned} \quad (2.35)$$

and the partition function of the system will be

$$\begin{aligned} Z &= \sum e^{-\beta H} = e^{-\beta E_0} \sum_{N_{\uparrow}, N_{\downarrow}} e^{-\beta \sum_k E_{\mathbf{k}} (N_{\uparrow} + N_{\downarrow} - 1)} = e^{-\beta E_0} \prod_{\mathbf{k}} e^{\beta E_{\mathbf{k}}} \sum_{N_{\uparrow}} e^{-\beta E_{\mathbf{k}} N_{\uparrow}} \sum_{N_{\downarrow}} e^{-\beta E_{\mathbf{k}} N_{\downarrow}} \\ &= e^{-\beta E_0} \prod_{\mathbf{k}} e^{\beta E_{\mathbf{k}}} \left(1 + e^{-\beta E_{\mathbf{k}}} \right)^2 = e^{-\beta E_0} \prod_{\mathbf{k}} \left(2 \cosh \left(\frac{\beta E_{\mathbf{k}}}{2} \right) \right)^2 \end{aligned} \quad (2.36)$$

This expression may now be used to find the free energy of the system:

$$F = -\frac{1}{\beta} \ln(Z) = E_0 - 2k_B T \sum_{\mathbf{k}} \ln \left[2 \cosh \left(\frac{E_{\mathbf{k}}}{2k_B T} \right) \right]. \quad (2.37)$$

Chapter 3

Physical System

We consider a two-dimensional SNS-junction in the xy -plane and parallel to the x -axis, with the interfaces placed at $x = -L/2$ and $x = L/2$. The width of the junction is W , see figure 3.1. The quasiparticle waves are represented by the four-component vectors $\Psi(x, y) = (\vec{u}(x, y) \ \vec{v}(x, y))^T$ as used in the Bogoliubov equations (2.25). We consider s-wave superconductors such that the gap parameter, $\Delta(x)$, is position-independent in each superconductor. The left and right superconductors are assumed to be of the same material, so that the magnitude, Δ , of the gap parameter is the same in both superconductors. However, we allow the gap parameter to have different phases, ϕ_L and ϕ_R , in the left and right superconductor, respectively. Necessarily, the gap parameter is zero in the normal metal. The overall gap parameter is

$$\Delta(x) = \Delta \left(e^{i\phi_L} \Theta(-L/2 - x) + e^{i\phi_R} \Theta(x - L/2) \right), \quad (3.1)$$

where $\Theta(x)$ is the Heaviside step function. The Hamiltonian will be on the form given in equation (2.20). We allow for different chemical potential, μ_S and μ_N , but we assume the effective mass to be equal in the superconductor and the normal metal, i.e. $m_S = m_N \equiv m$. Moreover, we let $V(x)$ be a delta-potential barrier at the interfaces and allow for different strength, i.e. $V(x) = V_L \delta(x + L/2) + V_R \delta(x - L/2)$. The overall Hamiltonian is

$$h(x, y) = h_S(x, y) (\Theta(-L/2 - x) + \Theta(x - L/2)) + h_N(x, y) \Theta(x + L/2) \Theta(L/2 - x) + V_L \delta(x) + V_R \delta(x - L) \quad (3.2)$$

where the Hamiltonian in the superconductors (S) and normal metal (N) is given as

$$h_{S/N}(x, y) = \frac{1}{2m} (-i\hbar\nabla - q\mathbf{A}(x, y))^2 - \mu_{S/N} \quad (3.3)$$

and \mathbf{A} is the vector potential allowing for an external magnetic field.

We will consider the semiclassical limit $k_F L \gg 1$, in which the Andreev bound states can be associated with classical trajectories, as illustrated in figure 3.1. These trajectories can be thought of as single-mode waveguides connecting the two superconductors !!!REF!!!. We will focus the circular Fermi surface with isotropic dependence on the wave vector $\mathbf{k} = (k_x, k_y) = (k_F \cos \theta_k, k_F \sin \theta_k)$. We will work in the short-junction regime $L \ll \xi$, with $\xi = \hbar v_f / \Delta$ the superconducting coherence length induced by the proximity effect !!!CITE!!!.

In the preceding chapters we will look at three different situations. First, in section 4.1 and 5.1, we will consider the system without external field or barriers at the interfaces. Next, in section 4.2 and 5.2, we will include the barriers at each interface, but keep the external field off. Finally, in section 4.3 and 5.3, we will include an external field, but have transparent barriers. The situations without the external field is well known !!!REF!!! and will be used for comparison. There has also been research on the situation with a uniform external magnetic field, both for one-dimensional and two-dimensional systems !!!REF!!!. However, we will also consider modulated magnetic fields, which has not yet been explored. Our strategy in all three situations is to first find the ABS-energies (chapter 4) and use this result to find the Josephson current (chapter 5).

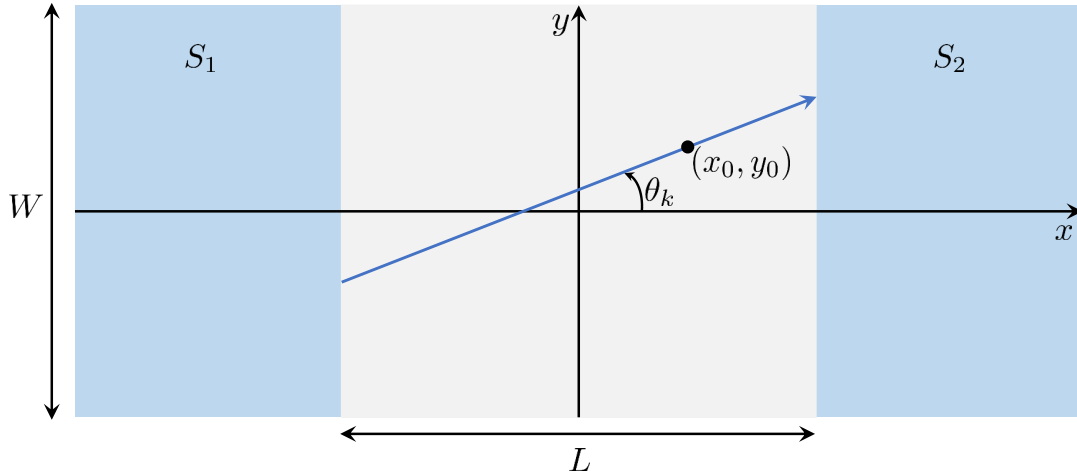


Figure 3.1: A Josephson junction formed by two superconductors of phase difference $\Delta\varphi$ connected by a normal metal of length L and width W . An electron trajectory used for semiclassical calculations of the supercurrent density at (x_0, y_0) is indicated.

Chapter 4

Andreev Bound State energies in SNS-junction

We will in this chapter find the ABS energies in the three situations described in chapter 3. For the situations without barriers at the interfaces the Andreev bound states will accumulate phase shifts as it travels along the classical trajectory described in chapter 3. This allow us to use the Bohr-Sommerfeld quantization condition !!!CITE!!! to find the ABS energies. When we include barriers the Andreev reflections can not be expressed as phase shifts and we must find the energies by setting up the wave-functions in each region and use boundary conditions to solve the system.

4.1 ABS energies without barriers or applied field

We will first consider the system with no applied field ($A = 0$) and no barriers ($V_L = V_R = 0$). We will first find the phase shift accumulated over a penetration depth in the superconductor when an electron or a hole is Andreev reflected at the NS-interface. Adding this to the phase accumulated when the electron or hole is traveling along the trajectory in figure 3.1, the total phase shift of the Andreev bound state is found and the Bohr-Sommerfeld quantization condition can be used to find the energies.

4.1.1 Andreev reflection amplitude

The probability amplitudes from chapter section 2.3 may be found by using the boundary conditions at the interface between the normal metal and the super conductor. With no barriers

the boundary conditions yields

$$\begin{aligned}\psi_i(0, y) + \psi_r(0, y) &= \psi_t(0, y) \\ \frac{\partial}{\partial x} \psi_i(0, y) + \frac{\partial}{\partial x} \psi_r(0, y) &= \frac{\partial}{\partial x} \psi_t(0, y).\end{aligned}\tag{4.1}$$

We insert the wave functions given in equation (??) in the boundary conditions and solve the system. The resulting amplitudes are given as

$$\begin{aligned}r_{eh} &= \frac{2e^{-i\varphi}}{\frac{u_0}{v_0} \frac{k_x^- + q_x^-}{k_x^+ + k_x^-} \left(1 + \frac{k_x^+}{q_x^+}\right) + \frac{v_0}{u_0} \frac{k_x^+ - q_x^-}{k_x^+ + k_x^-} \left(1 - \frac{k_x^-}{k_x^+}\right)} \\ r_{ee} &= \left(\frac{u_0}{v_0} \frac{k_x^+ + q_x^-}{k_x^+ + k_x^-} + \frac{v_0}{u_0} \frac{k_x^+ - q_x^-}{k_x^+ + k_x^-}\right) e^{i\varphi} r_{eh} \\ t_{ee} &= \frac{1}{v_0} \frac{k_x^- + q_x^-}{k_x^+ + k_x^-} e^{-i\beta} r_{eh} \\ t_{eh} &= \frac{1}{u_0} \frac{k_x^+ - q_x^-}{k_x^+ + k_x^-} e^{i\alpha} r_{eh},\end{aligned}\tag{4.2}$$

where $\varphi = \alpha - \beta$ is the phase of the gap parameter as shown in section 2.2.3. Since we are considering Andreev Bound States we are especially interested in the r_{eh} -amplitude, and see that it's expression may be simplified in the Andreev approximation !!!CITE!!! in which we let $k_x^\pm \approx q_x^\pm$:

$$r_{eh} = \frac{v_0}{u_0} e^{-i\varphi} \equiv e^{-i\eta} e^{-i\varphi},\tag{4.3}$$

where η is as defined in equation (2.18). Similarly, the amplitude of an incoming hole which is Andreev reflected as an electron will be $r_{he} = r_{eh}^*$:

$$r_{he} = \frac{v_0}{u_0} e^{i\varphi} = e^{-i\eta} e^{i\varphi}.\tag{4.4}$$

Hence, the Andreev reflection give a phase shift of $-\eta \mp \varphi$, where we use the upper (lower) sign if the incoming particle is an electron (hole) .

4.1.2 Bohr-Sommerfeld quantization

In the short junction regime, the continuous quasiparticle excitation spectrum ($E_{\mathbf{k}} < \Delta$) will not contribute to the Josephson current !!!CITE!!! and it is sufficient to restrict our selves to energies below the gap $E_{\mathbf{k}} < \Delta$ which yields $\eta = \arccos(E_{\mathbf{k}}/\Delta)$, according to equation(2.18). The Bohr-Sommerfeld quantization condition require the total phase obtained by the state in a whole cycle to be a multiple of 2π . REFERANSE. An electron starting at the left interface traveling to-

wards the right interface along a trajectory at an angle θ , see figure 3.1, would gain a phase of $L(k_x^+ + k_y^+ \tan \theta)$, before it is Andreev reflected at the right interface with the amplitude r_{eh} and thus is gaining a phase of $-\eta - \varphi$. The state would then continue as a hole traveling back along the same trajectory, accumulating a phase of $-L(k_x^- + k_y^- \tan \theta)$. Hence, the total phase in the quantization condition yields

$$\begin{aligned} 2\pi n = \oint d\phi &= \int_L^R \pm \mathbf{k}^\pm \cdot d\mathbf{l} + \phi_{(eh)(he)}^R + \int_R^L \pm \mathbf{k}^\mp \cdot d\mathbf{l} + \phi_{(he)(eh)}^L \\ &= L(k_x^+ - k_x^-) + L \tan \theta (k_y^+ - k_y^-) - 2\eta \pm \Delta\varphi \end{aligned} \quad (4.5)$$

where $\phi_{(eh)(he)}^{R/L} = -\eta \mp \varphi_{R/L}$ is the phase from Andreev reflection of an electron (hole) and we have defined the phase difference $\Delta\varphi \equiv \varphi_L - \varphi_R$. The upper sign indicate that the state starts out as a right-going electron, while the lower sign indicate that it starts as a right-going hole. Again we use the Andreev approximation and let $k_x^+ \approx k_x^-$ and $k_y^+ \approx k_y^-$ such that the two first terms vanish and the quantization condition is simply

$$2\pi n = -2\eta \pm \Delta\varphi. \quad (4.6)$$

4.1.3 ABS energy

Inserting equation (2.18) in the quantization condition above (4.6) we find the Andreev energy levels

$$E_{\mathbf{k}} = \Delta \cos \eta = \Delta \cos \left(\frac{\Delta\varphi}{2} \right). \quad (4.7)$$

This is the well known result in a SNS Josephson junction !!!CITE!!!.

4.2 ABS energies with barriers

We will in this section allow for barriers. Then the Andreev reflection amplitude will be more complicated so that we can not express it as a phase shift like we did above. We will instead find the energies by setting up the wave-functions in each region, insert the wave-functions in the boundary conditions and solve the system. The Hamiltonian of the system will be as given in equation (3.2), but with no external field so that we can set \mathbf{A} to zero. Hence,

$$h_{S/N}(x, y) = -\hbar^2 \nabla^2 / 2m - \mu_{S/N}. \quad (4.8)$$

4.2.1 Boundary conditions

Charge conservation yields continuous wave-functions at the interfaces:

$$\begin{aligned}\Psi_L(-L/2, y) &= \Psi_N(-L/2, y) \equiv \Psi(-L/2, y), \\ \Psi_R(L/2, y) &= \Psi_N(L/2, y) \equiv \Psi(L/2, y).\end{aligned}\tag{4.9}$$

We find the boundary conditions for the derivatives by integrating the BdG-equations (2.25):

$$\begin{aligned}0 &= \lim_{\epsilon \rightarrow 0} \int_{-L/2-\epsilon}^{-L/2+\epsilon} E_{\mathbf{k}} \Psi(x, y) dx = \lim_{\epsilon \rightarrow 0} \int_{-L/2-\epsilon}^{-L/2+\epsilon} \begin{pmatrix} \hat{H}(x, y) & \hat{\Delta}(x) \\ \hat{\Delta}^\dagger(x) & -\hat{H}(x, y) \end{pmatrix} \Psi(x, y) dx \\ &= \lim_{\epsilon \rightarrow 0} \int_{-L/2-\epsilon}^{-L/2^-} \begin{pmatrix} h_S(x, y) \hat{\sigma}_0 & i\Delta(x) \hat{\sigma}_2 \\ -i\Delta^*(x) \hat{\sigma}_2 & -h_S(x, y) \hat{\sigma}_0 \end{pmatrix} \Psi_L(x, y) dx + \begin{pmatrix} V_L \hat{\sigma}_0 & 0 \\ 0 & -V_L \hat{\sigma}_0 \end{pmatrix} \Psi(-L/2, y) \\ &\quad + \lim_{\epsilon \rightarrow 0} \int_{-L/2^+}^{-L/2+\epsilon} \begin{pmatrix} h_N(x) \hat{\sigma}_0 & 0 \\ 0 & -h_S(x) \hat{\sigma}_0 \end{pmatrix} \Psi_N(x, y) dx \\ &= \begin{pmatrix} \hat{\sigma}_0 & 0 \\ 0 & -\hat{\sigma}_0 \end{pmatrix} \left(V_L \Psi(-L/2, y) - \frac{\hbar^2}{2m} \lim_{\epsilon \rightarrow 0} \left(\int_{-L/2-\epsilon}^{-L/2^-} \frac{\partial^2}{\partial x^2} \Psi_L(x, y) dx + \int_{-L/2^+}^{-L/2+\epsilon} \frac{\partial^2}{\partial x^2} \Psi_N(x, y) dx \right) \right) \\ &= \begin{pmatrix} \hat{\sigma}_0 & 0 \\ 0 & -\hat{\sigma}_0 \end{pmatrix} \left(V_L \Psi(-L/2, y) - \frac{\hbar^2}{2m} \left(\frac{\partial \Psi_N}{\partial x} \Big|_{x=-L/2} - \frac{\partial \Psi_L}{\partial x} \Big|_{x=-L/2} \right) \right),\end{aligned}$$

and the boundary condition at the left interface for the derivatives is thus

$$\frac{\partial \Psi_N}{\partial x} \Big|_{x=-L/2} - \frac{\partial \Psi_L}{\partial x} \Big|_{x=-L/2} = \frac{2m}{\hbar^2} V_L \Psi(-L/2, y).\tag{4.10}$$

Similarly, we get

$$\frac{\partial \Psi_R}{\partial x} \Big|_{x=L/2} - \frac{\partial \Psi_N}{\partial x} \Big|_{x=L/2} = \frac{2m}{\hbar^2} V_R \Psi(L/2, y).\tag{4.11}$$

as boundary condition at the right interface.

4.2.2 Wave functions in the superconduction region

The solution of the BdG-equations (2.25) that satisfy the boundary conditions will be on the form

$$\Psi_{\mathbf{k}^\pm}(\mathbf{r}) = \begin{pmatrix} \vec{u}_{\mathbf{k}} \\ \vec{v}_{\mathbf{k}} \end{pmatrix} e^{i\mathbf{k}^\pm \cdot \mathbf{r}}.\tag{4.12}$$

Inserting the wavefunctions of this form in the time-independent Schrödinger equation yields

$$h(\mathbf{r}) \Psi_{\mathbf{k}^\pm}(\mathbf{r}) = \left(\frac{\hbar^2 k^{\pm 2}}{2m} - \mu \right) \Psi_{\mathbf{k}^\pm}(\mathbf{r}) \equiv \varepsilon_k^\pm \Psi_{\mathbf{k}^\pm}(\mathbf{r}),\tag{4.13}$$

where we let $h(\mathbf{r}) = h_S(x, y)$ as given in (4.8) in the superconducting region. For the eigenvalue problem in the BdG-equations (2.25) we must calculate

$$\begin{aligned} 0 &= \det \begin{pmatrix} (\varepsilon_{\mathbf{k}}^{\pm} - E_{\mathbf{k}}) \hat{\sigma}_0 & i\Delta \hat{\sigma}_2 \\ -i\Delta^* \hat{\sigma}_2 & (-\varepsilon_{\mathbf{k}}^{\pm} - E_{\mathbf{k}}) \hat{\sigma}_0 \end{pmatrix} \\ &= (\varepsilon_{\mathbf{k}}^{\pm} - E_{\mathbf{k}})^2 \left(\varepsilon_{\mathbf{k}}^{\pm} + E_{\mathbf{k}} + \frac{\Delta^2}{\varepsilon_{\mathbf{k}}^{\pm} - E_{\mathbf{k}}} \right)^2. \end{aligned} \quad (4.14)$$

As $E_{\mathbf{k}} = \varepsilon_{\mathbf{k}}^{\pm}$ would give zero in the denominator when Δ is non-zero, the only solution to the above equation (4.14) is

$$E_{\mathbf{k}}^2 = \varepsilon_{\mathbf{k}}^{\pm 2} + \Delta^2 \quad (4.15)$$

which agrees with the energies obtained in equation (2.16). k^{\pm} and $\varepsilon_{\mathbf{k}}^{\pm}$ will be as in equation (2.17) and we will only consider positive energies, $E_{\mathbf{k}} = \sqrt{\varepsilon_{\mathbf{k}}^{\pm 2} + \Delta^2}$. For $\varepsilon_{\mathbf{k}}^+ = +\sqrt{E_{\mathbf{k}}^2 - \Delta^2} = i\Delta \sin \eta$ we get the (non-normalized) wave-functions describing electronlike quasiparticles:

$$\Psi_{e,\uparrow}^{\pm}(x, y) = \begin{pmatrix} e^{i(\eta+\varphi)} \\ 0 \\ 0 \\ 1 \end{pmatrix} e^{i(\pm k_x^+ x + k_y^+ y)} \quad \text{and} \quad \Psi_{e,\downarrow}^{\pm}(x, y) = \begin{pmatrix} 0 \\ e^{i(\eta+\varphi)} \\ -1 \\ 0 \end{pmatrix} e^{i(\pm k_x^+ x + k_y^+ y)}, \quad (4.16)$$

where $\Psi_{e,\sigma}^+$ are right-going waves, while $\Psi_{e,\sigma}^-$ are left-going waves. Similarly, for $\varepsilon_{\mathbf{k}}^- = -\sqrt{E_{\mathbf{k}}^2 - \Delta^2} = -i\Delta \sin \eta$ we get the wave-functions describing holelike quasiparticles:

$$\Psi_{h,\uparrow}^{\pm}(x, y) = \begin{pmatrix} 1 \\ 0 \\ 0 \\ e^{i(\eta-\varphi)} \end{pmatrix} e^{i(\pm k_x^- x + k_y^- y)} \quad \text{and} \quad \Psi_{h,\downarrow}^{\pm}(x, y) = \begin{pmatrix} 0 \\ -1 \\ e^{i(\eta-\varphi)} \\ 0 \end{pmatrix} e^{i(\pm k_x^- x + k_y^- y)}, \quad (4.17)$$

where $\Psi_{h,\sigma}^+$ are left-going waves, while $\Psi_{h,\sigma}^-$ are right-going waves. The direction of the waves is determined from the group velocity:

$$\mathbf{v}_g = \frac{1}{\hbar} \frac{\partial E_{\mathbf{k}}}{\partial \mathbf{k}} = \frac{\varepsilon_{\mathbf{k}}^{\pm}}{E_{\mathbf{k}}} \frac{\hbar \mathbf{k}^{\pm}}{m}. \quad (4.18)$$

We allow for different phases, φ_L and φ_R , in each region. As we will only consider energies below the gap, $E_{\mathbf{k}} < \Delta$, the wave vectors (2.17) will get imaginary parts and must vanish in the superconductors. Consequently there will be no incoming wave-functions from the superconductor into the normal metal with such energies and we need only to consider the outgoing wave-

functions in the superconducting regions. We let $k_y^+ \approx k_y^- \equiv k_y$ and the total wave functions in the left (L) and right (R) region will thus be

$$\begin{aligned}\Psi_L(x - L/2, y) &= \Psi_L(x - L/2) e^{ik_y y} \\ \Psi_R(x + L/2, y) &= \Psi_R(x + L/2) e^{ik_y y}\end{aligned}\quad (4.19)$$

with $\Psi_{L/R}(x \mp L/2)$ defined as

$$\begin{aligned}\Psi_L(x - L/2) &= a_1 \begin{pmatrix} e^{i(\eta+\varphi_L)} \\ 0 \\ 0 \\ 1 \end{pmatrix} e^{-ik_x^+ x} + a_2 \begin{pmatrix} 0 \\ e^{i(\eta+\varphi_L)} \\ -1 \\ 0 \end{pmatrix} e^{-ik_x^+ x} + a_3 \begin{pmatrix} 1 \\ 0 \\ 0 \\ e^{i(\eta-\varphi_L)} \end{pmatrix} e^{ik_x^- x} + a_4 \begin{pmatrix} 0 \\ -1 \\ e^{i(\eta-\varphi_L)} \\ 0 \end{pmatrix} e^{ik_x^- x} \\ \Psi_R(x + L/2) &= b_1 \begin{pmatrix} e^{i(\eta+\varphi_R)} \\ 0 \\ 0 \\ 1 \end{pmatrix} e^{ik_x^+ x} + b_2 \begin{pmatrix} 0 \\ e^{i(\eta+\varphi_R)} \\ -1 \\ 0 \end{pmatrix} e^{ik_x^+ x} + b_3 \begin{pmatrix} 1 \\ 0 \\ 0 \\ e^{i(\eta-\varphi_R)} \end{pmatrix} e^{-ik_x^- x} + b_4 \begin{pmatrix} 0 \\ -1 \\ e^{i(\eta-\varphi_R)} \\ 0 \end{pmatrix} e^{-ik_x^- x}.\end{aligned}\quad (4.20)$$

We have here absorbed a phase factor $\exp(\pm ik_x L/2)$ in the coefficients in order to simplify the boundary equations.

4.2.3 Wave functions in the normal region

In the normal region the gap parameter, $\Delta(x)$, is zero, and so $u_0 = 1$ and $v_0 = 0$ and the eigenvalues are E_k such that $\varepsilon_k^\pm = \pm E_k$. The corresponding eigenvectors are

$$\Psi_{e,\uparrow}(\mathbf{r}) = \begin{pmatrix} 1 \\ 0 \\ 0 \\ 0 \end{pmatrix} e^{i\mathbf{k}^+ \cdot \mathbf{r}}, \quad \Psi_{e,\downarrow}(\mathbf{r}) = \begin{pmatrix} 0 \\ 1 \\ 0 \\ 0 \end{pmatrix} e^{i\mathbf{k}^+ \cdot \mathbf{r}}, \quad \Psi_{h,\uparrow}(\mathbf{r}) = \begin{pmatrix} 0 \\ 0 \\ 1 \\ 0 \end{pmatrix} e^{i\mathbf{k}^- \cdot \mathbf{r}}, \quad \Psi_{h,\downarrow}(\mathbf{r}) = \begin{pmatrix} 0 \\ 0 \\ 0 \\ 1 \end{pmatrix} e^{i\mathbf{k}^- \cdot \mathbf{r}}. \quad (4.21)$$

We must here allow both right- and leftgoing waves and the total wave function in the normal region becomes

$$\Psi_N(x - L/2, y) = \Psi_N(x - L/2) e^{ik_y y} \quad (4.22)$$

with

$$\Psi_N(x - L/2) = c_1 \begin{pmatrix} 1 \\ 0 \\ 0 \\ 0 \end{pmatrix} e^{ik^+ x} + c_2 \begin{pmatrix} 1 \\ 0 \\ 0 \\ 0 \end{pmatrix} e^{-ik^+ x} + c_3 \begin{pmatrix} 0 \\ 1 \\ 0 \\ 0 \end{pmatrix} e^{ik^+ x} + c_4 \begin{pmatrix} 0 \\ 1 \\ 0 \\ 0 \end{pmatrix} e^{-ik^+ x} \\ + c_5 \begin{pmatrix} 0 \\ 0 \\ 1 \\ 0 \end{pmatrix} e^{ik^- x} + c_6 \begin{pmatrix} 0 \\ 0 \\ 1 \\ 0 \end{pmatrix} e^{-ik^- x} + c_7 \begin{pmatrix} 0 \\ 0 \\ 0 \\ 1 \end{pmatrix} e^{ik^- x} + c_8 \begin{pmatrix} 0 \\ 0 \\ 0 \\ 1 \end{pmatrix} e^{-ik^- x}. \quad (4.23)$$

4.2.4 ABS energy

We use the boundary conditions found in section 4.2.1:

$$\begin{aligned} \Psi_L(-L/2) - \Psi_N(-L/2) &= 0 \\ \Psi_R(L/2) - \Psi_N(L/2) &= 0 \\ \frac{\partial \Psi_N(x)}{\partial x} \Big|_{x=-L/2} - \frac{\partial \Psi_L(x)}{\partial x} \Big|_{x=-L/2} - Z_L k_x \Psi_L(-L/2) &= 0 \\ \frac{\partial \Psi_R(x)}{\partial x} \Big|_{x=L/2} - \frac{\partial \Psi_N(x)}{\partial x} \Big|_{x=L/2} - Z_R k_x \Psi_R(L/2) &= 0 \end{aligned} \quad (4.24)$$

and insert the equations in a homogeneous matrix equation of the form

$$M(a_1 \cdots a_4 \ b_1 \cdots b_4 \ c_1 \cdots c_8)^T = 0 \quad (4.25)$$

where M is a 16×16 -matrix. We have let $k_x^+ \approx k_x^- \equiv k_x$ and defined the barrier strengths

$$Z_L = \frac{2mV_L}{\hbar^2 k_x^2} \quad \text{and} \quad Z_R = \frac{2mV_R}{\hbar^2 k_x^2}. \quad (4.26)$$

The determinant of M is found to be

$$\det(M) = \left(8e^{i\eta}\right)^4 \left[\sin^2 \frac{\Delta\varphi}{2} - (1 + \zeta) \sin^2 \eta \right]^2 \quad (4.27)$$

which must be zero in order for the equations to have non-trivial solutions. Hence, the energy is

$$E = \Delta \cos \eta = \Delta \sqrt{\frac{\cos^2 \frac{\Delta\varphi}{2} + \zeta}{\zeta + 1}}. \quad (4.28)$$

We have again let $\Delta\varphi = \varphi_L - \varphi_R$ be the phase difference between the left and right semiconductor. We have also introduced ζ which measures the effect of the barriers and is given as

$$\zeta = Z^2 + z^2 \sin(k_F L) \left[Z \cos(k_F L) + \left(\frac{z^2}{4} - 1 \right) \sin(k_F L) \right] \quad (4.29)$$

where Z and z are defined as

$$Z = \frac{Z_L + Z_R}{2} \quad \text{and} \quad z = \sqrt{Z_L Z_R}. \quad (4.30)$$

In the limit with no barrier, i.e. $\zeta = 0$ we see that equation (4.28) yields (4.7).

4.3 ABS energies with applied field

We will now apply a magnetic field, \vec{B} , to the junction, and let the barriers be transparent. This imply modifying the Hamiltonian to

$$h_N(\mathbf{r}) = \frac{1}{2m_N} \left(\frac{\hbar}{i} \nabla - q\mathbf{A}(\mathbf{r}) \right)^2 + q\varphi - \mu_N \quad (4.31)$$

with $\mathbf{A}(\mathbf{r})$ as the vector potential and φ as the scalar potential.

Our strategy now is the same as in section 4.1. We want to express the problem in the phase of the wave function and use the quantization condition to find the energy.

4.3.1 Guage transformation

As we must have Gauge invariance we may do the transformation

$$\begin{aligned} \mathbf{A}' &= \mathbf{A} + \nabla f \\ \varphi' &= \varphi - \frac{\partial f}{\partial t} \end{aligned} \quad (4.32)$$

where f is any function of position and time. Doing such transformation imply a transformation in the wavefunction Ψ as well. Considering the time-dependent Schrödinger equation yields

$$\begin{aligned} i\hbar \frac{\partial \Psi}{\partial t} &= \left[\frac{1}{2m} \left(\frac{\hbar}{i} \nabla - q\mathbf{A}' \right)^2 + q\varphi' - \mu_N \right] \Psi \\ &= \left[\frac{1}{2m} \left(\frac{\hbar}{i} \nabla - q\mathbf{A}' + q\nabla f \right)^2 + q\varphi' + q \frac{\partial f}{\partial t} - \mu_N \right] \Psi, \end{aligned} \quad (4.33)$$

giving

$$i\hbar \frac{\partial \Psi}{\partial t} - q \frac{\partial f}{\partial t} \Psi = \left[\frac{1}{2m} \left(\frac{\hbar}{i} \nabla - q\mathbf{A}' + q\nabla f \right)^2 + q\varphi' - \mu_N \right] \Psi \quad (4.34)$$

or

$$\begin{aligned} i\hbar \frac{\partial}{\partial t} \left(\Psi e^{iqf/\hbar} \right) &= e^{iqf/\hbar} \left[\frac{1}{2m} \left(\frac{\hbar}{i} \nabla - q\mathbf{A}' + q\nabla f \right)^2 + q\varphi' \right] \Psi \\ &= \left[\frac{1}{2m} \left(\frac{\hbar}{i} \nabla - q\mathbf{A}' \right)^2 + q\varphi' \right] \left(\Psi e^{iqf/\hbar} \right), \end{aligned} \quad (4.35)$$

where we have used that

$$e^{iqf/\hbar} \left(\frac{\hbar}{i} \nabla + q\nabla f \right) \Psi = \frac{\hbar}{i} \nabla \left(e^{iqf/\hbar} \Psi \right). \quad (4.36)$$

The Schrödinger equation in the transformed system is now on the same form as the original system:

$$i\hbar \frac{\partial \Psi'}{\partial t} = \left[\frac{1}{2m} \left(\frac{\hbar}{i} \nabla - q\mathbf{A}' \right)^2 + q\varphi' \right] \Psi' \quad (4.37)$$

with $\Psi' = e^{iqf/\hbar} \Psi$. Thus a Gauge transformation $\mathbf{A} \rightarrow \mathbf{A} + \nabla\chi$ imply a transformation $\phi \rightarrow \phi + q\chi/\hbar$ in the phase.

A Gauge invariant phase will be on the form

$$\phi_{GI} = \phi - \frac{q}{\hbar} \int \mathbf{A} \cdot d\mathbf{r}, \quad (4.38)$$

as transformation $\phi \rightarrow \phi + q\chi/\hbar$ and $\mathbf{A} \rightarrow \mathbf{A} + \nabla\chi$ give

$$\begin{aligned} \phi_{GI} &\rightarrow \phi + \frac{q}{\hbar}\chi - \frac{q}{\hbar} \int (\mathbf{A} + \nabla\chi) \cdot d\mathbf{r} = \phi - \frac{q}{\hbar} \int \mathbf{A} \cdot d\mathbf{r} + \frac{q}{\hbar}\chi - \frac{q}{\hbar}\chi \\ &= \phi - \frac{q}{\hbar} \int \mathbf{A} \cdot d\mathbf{r}. \end{aligned} \quad (4.39)$$

We have in the previous sections taken \mathbf{A} to be zero so that $\phi_{GI} = \phi$. However, now we must include the vector potential in the phase as the magnetic field is non-zero.

4.3.2 Bohr-Sommerfeld quantization condition

Using the same method as in equation (4.6), but with the Gauge invariant phase we get the quantization condition

$$\begin{aligned} 2\pi n &= \oint d\phi = \int_L^R \pm \mathbf{k}^\pm \cdot d\mathbf{l} \pm \frac{e}{\hbar} \int_L^R \mathbf{A} \cdot d\mathbf{l} + \phi_{(eh)(he)}^R + \int_R^L \pm \mathbf{k}^\mp \cdot d\mathbf{l} \mp \frac{e}{\hbar} \int_R^L \mathbf{A} \cdot d\mathbf{l} + \phi_{(he)(eh)}^L \\ &= L(k_x^+ - k_x^-) + L \tan \theta (k_y^+ - k_y^-) - 2\eta \pm \left(\Delta\varphi + \frac{2e}{\hbar} \int_L^R \mathbf{A} \cdot d\mathbf{l} \right). \end{aligned} \quad (4.40)$$

Again, we let $k_x^+ \approx k_x^-$ and $k_y^+ \approx k_y^-$ and are left with

$$2\pi n = -2\eta \pm (\Delta\varphi - \gamma), \quad (4.41)$$

where we have defined

$$\gamma = -\frac{2e}{\hbar} \int_L^R \mathbf{A} \cdot d\mathbf{l}. \quad (4.42)$$

We have assumed the curvature of the electrons, due to the Lorentz force, to be much larger than the length of the junction, so that we can neglect the effect the field has on the trajectory of the electrons/holes.

4.3.3 ABS energy

The energy is then

$$E_{\mathbf{k}} = \Delta \cos \eta = \Delta \cos \left(\frac{\Delta\varphi}{2} - \frac{\gamma}{2} \right). \quad (4.43)$$

We see that when the the field is zero, i.e. $\gamma = 0$, we get the same expression as equation (4.7).

Chapter 5

Andreev Bound State Current in SNS-junction

In chapter 2.4 we saw how the Josephson current can be expressed in terms of the free energy and phase difference between the two superconductors (2.32). In chapter 2.5 we expressed the free energy in terms of the energy levels, $E_{\mathbf{k}}$. Using equation (2.32) and (2.37) we can thus express the Josephson current in terms of the ABS energy and the phase difference:

$$\begin{aligned} I_x(\Delta\varphi) &= \sum_{k_y} \delta I(\mathbf{r}, \mathbf{k}) \rightarrow \int dy \int \frac{dk_y}{2\pi} \delta I(\mathbf{r}, \mathbf{k}), \\ I_y(\Delta\varphi) &= \sum_{k_x} \delta I(\mathbf{r}, \mathbf{k}) \rightarrow \int dx \int \frac{dk_x}{2\pi} \delta I(\mathbf{r}, \mathbf{k}), \end{aligned} \quad (5.1)$$

where we have defined

$$\delta I(\mathbf{r}, \mathbf{k}) \equiv -\frac{2e}{\hbar} \tanh\left(\frac{E_{\mathbf{k}}}{2k_B T}\right) \frac{\partial E_{\mathbf{k}}}{\partial(\Delta\varphi)} \quad (5.2)$$

and I_y should be zero due to current conservation. The current density will be given as

$$\begin{aligned} j_x(x, y) &= \int \frac{dk_y}{2\pi} \delta I(\mathbf{r}, \mathbf{k}) = \frac{k_F}{2\pi} \int_{-\pi/2}^{\pi/2} d\theta_k \cos\theta_k \delta I(\mathbf{r}, \mathbf{k}), \\ j_y(x, y) &= \int \frac{dk_x}{2\pi} \delta I(\mathbf{r}, \mathbf{k}) = \frac{k_F}{2\pi} \int_{-\pi/2}^{\pi/2} d\theta_k \sin\theta_k \delta I(\mathbf{r}, \mathbf{k}), \end{aligned} \quad (5.3)$$

where we have let

$$\begin{pmatrix} dk_x \\ dk_y \end{pmatrix} \rightarrow k_F \begin{pmatrix} \sin\theta_k \\ \cos\theta_k \end{pmatrix} d\theta_k \quad (5.4)$$

as we consider the circular Fermi surface, as stated in chapter 3.

In chapter 4 the ABS energy levels were found for the three different situations and we will in this chapter use these energies in equation (5.3) to find the current density and in equation (5.1) to find the total and critical current for each of the three situations. For the analytical progress we will consider the high temperature regime, ($k_B T \gtrsim \Delta$), in which the analytical calculations are simpler.

5.1 ABS current without barriers or applied field

In the case with no barriers or magnetic field we use equation (4.7) in equation (5.2) to obtain

$$\delta I = \frac{e\Delta}{\hbar} \sin\left(\frac{\Delta\varphi}{2}\right) \tanh\left(\frac{\Delta \cos(\Delta\varphi/2)}{2k_B T}\right), \quad (5.5)$$

which we notice is independent of the trajectory of the particle. From equation (5.3) one finds the current density to be zero in the y -direction, $j_y(x, y) = 0$, and uniform in the x -direction, $j_x(x, y) = I_x/W$, where W is the junction width (indicated in figure 3.1) and I_x as the total current:

$$I_x = k_F W \frac{e\Delta}{\pi\hbar} \sin\left(\frac{\Delta\varphi}{2}\right) \tanh\left(\frac{\Delta \cos(\Delta\varphi/2)}{2k_B T}\right). \quad (5.6)$$

In the high temperature regime ($k_B T \gtrsim \Delta$) this can be approximated to

$$I_x = k_F W \frac{e\Delta}{\pi\hbar} \sin\left(\frac{\Delta\varphi}{2}\right) \frac{\Delta \cos(\Delta\varphi/2)}{2k_B T} = I_{c,0} \sin \Delta\varphi \quad (5.7)$$

with

$$I_{c,0} = \frac{k_F W e \Delta^2}{4\pi\hbar k_B T} \quad (5.8)$$

as the high temperature critical current. These results are well known !!!CITE!!! and will be used for comparison in the preceding sections.

5.2 ABS current with barriers

The ABS energy levels in the case of no barriers was found in equation (4.28). Inserting this in equation (5.2) yields

$$\delta I = \frac{e\Delta}{2\hbar} \frac{\sin(\Delta\varphi)}{\sqrt{(\cos^2(\Delta\varphi/2) + \zeta)(\zeta + 1)}} \tanh\left(\frac{\Delta}{2k_B T} \sqrt{\frac{\cos^2(\Delta\varphi/2) + \zeta}{\zeta + 1}}\right). \quad (5.9)$$

Also here δI is independent of the trajectory such that the current density is uniform. The total current is

$$I_x = k_F W \frac{e\Delta}{2\pi\hbar} \frac{\sin(\Delta\varphi)}{\sqrt{(\cos^2(\Delta\varphi/2) + \zeta)(\zeta + 1)}} \tanh\left(\frac{\Delta}{2k_B T} \sqrt{\frac{\cos^2(\Delta\varphi/2) + \zeta}{\zeta + 1}}\right). \quad (5.10)$$

The high temperature critical current is

$$I_{c,\zeta} = \frac{k_F W e \Delta^2}{4\pi\hbar k_B T} \frac{1}{\zeta + 1} = \frac{I_{c,0}}{\zeta + 1}, \quad (5.11)$$

with $I_{c,0}$ is the critical current without barriers (5.8). Figure 5.1 shows how the total current varies with the phase difference, $\Delta\varphi$, in the high temperature regime ($k_B T = \Delta$) for different barrier strengths, ζ .

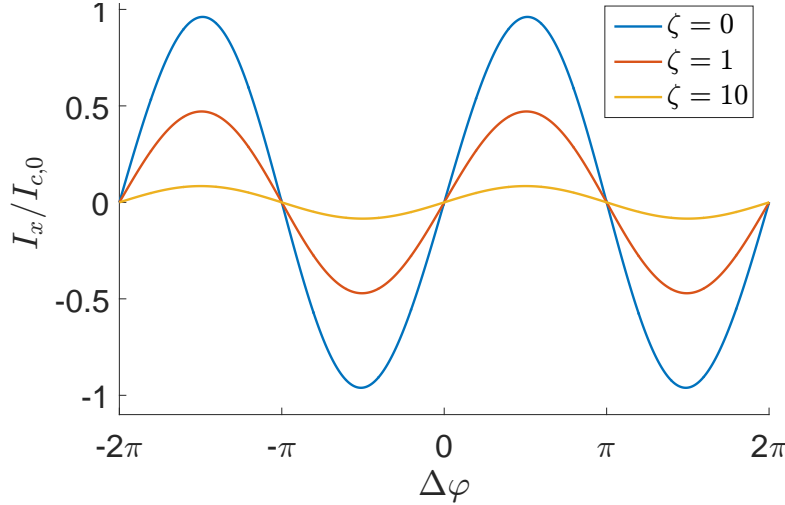


Figure 5.1: Plot of the total supercurrent I_x versus the superconducting phase difference $\Delta\varphi$ through the normal region of the Josephson junction at temperature $k_B T = \Delta$. The current is calculated from equation (5.10) for different barrier strengths, ζ , at the superconducting interface.

5.3 ABS current with applied field

With no barriers, but magnetic field we find the current from the ABS energy in equation (4.43):

$$\delta I_k(\Delta\varphi) = \frac{e\Delta}{\hbar} \sin\left(\frac{\Delta\varphi}{2} - \frac{\gamma_k}{2}\right) \tanh\left(\frac{\Delta \cos\left(\frac{\Delta\varphi}{2} - \frac{\gamma_k}{2}\right)}{2k_B T}\right) \quad (5.12)$$

which in the high temperature regime ($k_B T \gtrsim \Delta$), can be approximated to

$$\delta I_k(\Delta\varphi) \approx \frac{e\Delta^2}{4\hbar k_B T} \sin(\Delta\varphi - \gamma_k). \quad (5.13)$$

The Aharonov-Bohm phase shift, γ_k , will depend on the modulation and strength of the magnetic field, and on the trajectory of the particle. We will here consider three different modulations of the magnetic field. That is a uniform magnetic field (section 5.3.1), sinusoidal field varying along the junction (section 5.3.2) and sinusoidal field varying along the interfaces (section 5.3.3).

The magnetic field will be expelled in the superconducting region, due to the Meissner effect. We assume the penetration depth to be short even in the high-field regime, i.e. when $l_m \lesssim L$ with $l_m = \sqrt{\hbar/eB}$ as the magnetic length. The Lorentz effect will change the trajectories in the magnetic field into arcs of cyclotron radius $l_{\text{cycl}} = \hbar k_F/eB = k_F l_m^2$. However, we assume that $k_F L$ is sufficiently large such that $l_{\text{cycl}}/L = k_F L(l_m/L)^2 \gg 1$ for the fields considered and we can neglect the curvature of the trajectories.

5.3.1 Uniform magnetic field

We will first consider a uniform magnetic field of strength B :

$$\mathbf{B} = B [\Theta(x + L/2) - \Theta(x - L/2)] \hat{z}, \quad (5.14)$$

and choose the gauge of the \mathbf{A} -field as

$$\mathbf{A} = -By [\Theta(x + L/2) - \Theta(x - L/2)] \hat{x}. \quad (5.15)$$

The Aharonov-Bohm phase shift, $\gamma(x_0, y_0, \theta_k)$, is calculated from equation (4.42) by integration along a path through the point (x_0, y_0) at an angle θ_k with the x -axis, as shown in figure 3.1. The trajectory will be given by the line

$$y(x) = y_0 - x_0 \tan \theta_k + x \tan \theta_k. \quad (5.16)$$

Using this in equation (4.42) we find the phase shift:

$$\begin{aligned} \gamma &= -\frac{2e}{\hbar} \int_L^R \mathbf{A} \cdot d\mathbf{l} = B \frac{2e}{\hbar} \int_{-L/2}^{L/2} y(x) dx \\ &= \frac{2L}{l_m^2} (y_0 - x_0 \tan \theta_k). \end{aligned} \quad (5.17)$$

This expression is used in equation (5.12) and (5.3) in order to find the current density. The result from numerical computation is shown in figure 5.2 for three different magnetic lengths revealing the appearance of a row of current vortex-antivortex pairs. The distance, d_{vortex} , between two vortices placed at y_0 and $y_0 + d$ will satisfy the relation

$$\gamma(y_0 + d_{\text{vortex}}) = \gamma(y_0) + 2\pi \quad (5.18)$$

as this gives equal current density in the vortices according to equation (5.13). By inserting for γ we find the vortex distance

$$d_{\text{vortex}} = \pi \frac{l_m^2}{L}, \quad (5.19)$$

and it is clear that the distance between the vortices increases with the magnetic length, as observed in figure 5.2. In the figure we have chosen the phase difference to be $\Delta\varphi = \pi/2$. A change $\delta\varphi$ in $\Delta\varphi$ would give a shift along the y -axis:

$$\delta I_k(y_0, \Delta\varphi + \delta\varphi) = \delta I_k\left(y_0 - \frac{l_m^2}{2L}, \delta\varphi\right), \quad (5.20)$$

as we from equation (5.12) have

$$\delta I_k(y_0, \Delta\varphi + \delta\varphi) = \frac{e\Delta}{\hbar} \sin\left(\frac{\Delta\varphi}{2} - \frac{\gamma_k - \delta\varphi}{2}\right) \tanh\left(\frac{\Delta \cos\left(\frac{\Delta\varphi}{2} - \frac{\gamma_k - \delta\varphi}{2}\right)}{2k_B T}\right) \quad (5.21)$$

and

$$\gamma_k(y_0) - \delta\varphi = \frac{2L}{l_m^2} \left(y_0 - \frac{l_m^2}{2L} \delta\varphi - x_0 \tan\theta_k \right) = \gamma_k\left(y_0 - \frac{l_m^2}{2L} \delta\varphi\right). \quad (5.22)$$

However, the linear vortex pattern remains.

In order to find the total current we combine equation (5.1), (5.3) and (5.12):

$$I_x = \frac{k_F e \Delta}{2\pi \hbar} \int_{-W/2}^{W/2} dy_0 \int_{-\pi/2}^{\pi/2} d\theta_k \cos\theta_k \sin\left(\frac{\Delta\varphi}{2} - \frac{\gamma}{2}\right) \tanh\left(\frac{\Delta}{2k_B T} \cos\left(\frac{\Delta\varphi}{2} - \frac{\gamma}{2}\right)\right) \quad (5.23)$$

which in the high temperature regime ($k_B T \gtrsim \Delta$) is simplified to

$$I_x = \frac{I_{c,0}}{2W} \int_{-W/2}^{W/2} dy_0 \int_{\pi/2}^{\pi/2} d\theta_k \cos\theta_k \sin(\Delta\varphi - \gamma). \quad (5.24)$$

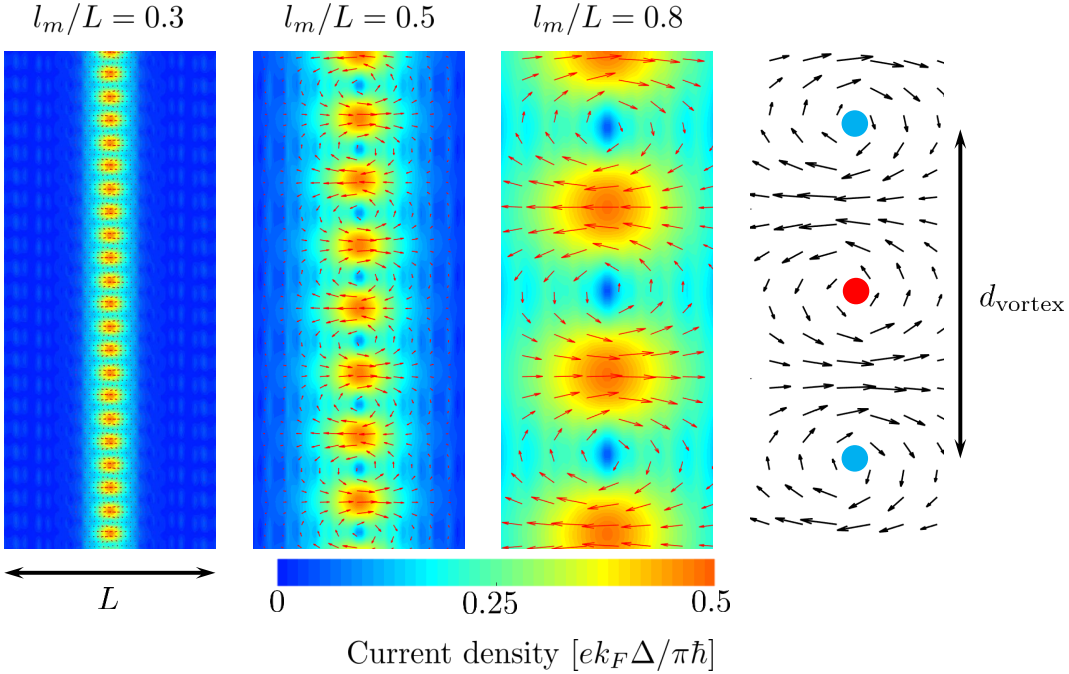


Figure 5.2: The three scale plots show the supercurrent density in a wide Josephson junction, far from the lateral boundaries for three values of the magnetic field. The plots are calculated numerically from equation (5.3), (5.12) and (5.17) at $k_B T = \Delta$. The current density of magnetic field $l_m/L = 0.8$ is also illustrated in the velocity plot to the right with vortices and anti-vortices indicated along with the vortex distance $d_{\text{vortex}} = \pi l_m^2/L$.

From equation (5.17) we notice that $\gamma(x_0, y_0, \theta_k) = -\gamma(x_0, -y_0, -\theta)$ which allows us to write

$$I_x = \frac{I_{c,0}}{W} \sin(\Delta\varphi) \int_{-W/2}^{W/2} dy_0 \int_0^{\pi/2} d\theta_k \cos\theta_k \cos\gamma. \quad (5.25)$$

The integral over y_0 gives

$$\int_{-W/2}^{W/2} dy_0 \cos\gamma = \frac{l_m^2}{L} \sin\left(\frac{LW}{l_m^2}\right) \cos\left(\frac{2L}{l_m^2} x_0 \tan\theta_k\right) \approx \frac{l_m^2}{L} \sin\left(\frac{LW}{l_m^2}\right), \quad (5.26)$$

where we the last equality is taken in the low field regime ($l_m \gg L$) in order to simplify the analytical expression. The total current is thus

$$I_x = I_{c,0} \frac{\sin\left(\frac{e}{\hbar}\Phi\right)}{\frac{e}{\hbar}\Phi} \sin\Delta\varphi \quad (5.27)$$

with $\Phi = BLW$ as the magnetic flux and we find the critical current at $\Delta\varphi = \pi/2$:

$$I_{c,\text{const}} = I_{c,0} \left| \frac{\sin\left(\frac{e}{\hbar}\Phi\right)}{\frac{e}{\hbar}\Phi} \right| \quad (5.28)$$

which is the well known Fraunhofer oscillations. By comparing the period $\Phi_0 = \pi\hbar/e$ with the vortex distance d_{vortex} from equation (5.19) we find the relation

$$d_{\text{vortex}} = W \frac{\Phi_0}{\Phi}. \quad (5.29)$$

The critical current resulting from numerical calculations is shown in figure 5.3.

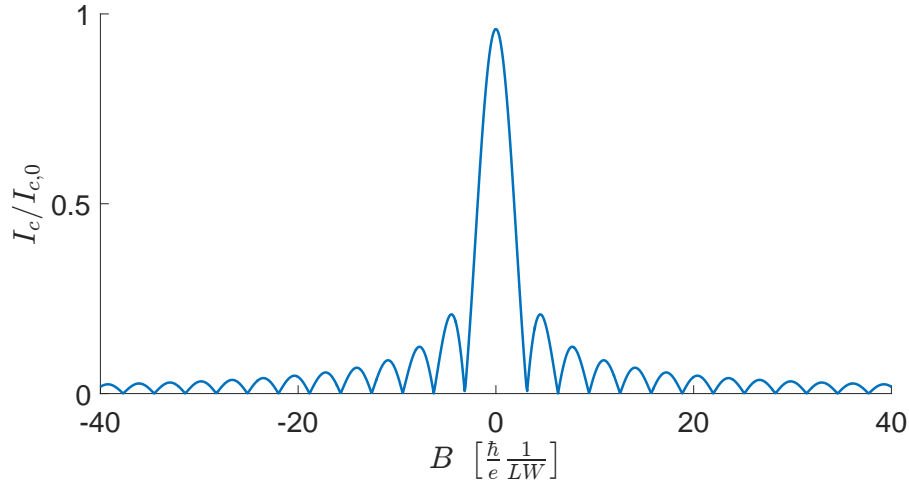


Figure 5.3: Plot of the critical current I_c through the normal region versus the magnetic field strength B in a uniform field. The current is calculated numerically from equation (5.1), (5.12) and (5.17) at $\Delta\varphi = \pi/2$.

5.3.2 Sinusoidal field varying along the junction

We will next consider a sinusoidal magnetic field along the junction:

$$\mathbf{B} = B \sin\left(\frac{2\pi}{\lambda}x + \varphi\right) [\Theta(x + L/2) - \Theta(x - L/2)] \hat{z} \quad (5.30)$$

with the gauge

$$\mathbf{A} = -By \sin\left(\frac{2\pi}{\lambda}x + \varphi\right) [\Theta(x + L/2) - \Theta(x - L/2)] \hat{x}. \quad (5.31)$$

Again we use (4.42) and integrate along the trajectory in (5.16) to find the Aharonov-Bohm phase shift:

$$\begin{aligned}\gamma &= \frac{2}{l_m^2} \int_{-L/2}^{L/2} y(x) \sin\left(\frac{2\pi}{\lambda} + \varphi\right) dx \\ &= \frac{2\lambda}{\pi l_m^2} \left([y_0 - x_0 \tan \theta_k] \sin\left(\frac{\pi L}{\lambda}\right) \sin \varphi + \frac{L}{2} \tan \theta_k \left[\frac{\lambda}{\pi L} \sin\left(\frac{\pi L}{\lambda}\right) - \cos\left(\frac{\pi L}{\lambda}\right) \right] \cos \varphi \right).\end{aligned}\quad (5.32)$$

Symmetric field

More specifically we let $\varphi = \pi/2$ in (5.30) so that the the magnetic field becomes symmetric about the y -axis and the second term in equation (5.32) is zero such that the phase shift is

$$\gamma = \frac{2\lambda}{\pi l_m^2} [y_0 - x_0 \tan \theta_k] \sin\left(\frac{\pi L}{\lambda}\right) = \gamma_{\text{uni}} \frac{\sin(\pi L/\lambda)}{\pi L/\lambda} \quad (5.33)$$

where γ_{uni} is the Aharonov-Bohm phase shift in the uniform magnetic field as given in equation (5.17). As this expression is proportional to the phase shift for uniform field we expect appearance of current vortices, but with a vortex distance dependent on the wavelength of the magnetic field:

$$d_{\text{vortex}} = \pi \frac{l_m^2}{L} \left| \frac{\pi L/\lambda}{\sin(\pi L/\lambda)} \right|. \quad (5.34)$$

Hence, the distance between the vortices can be controlled not only by changing the magnetic field strength, but also by changing the wavelength of the symmetric field. For wavelengths $\lambda = L/n$, with n as an non-zero integer, we notice that $d_{\text{vortex}} \rightarrow \infty$ and $\gamma \rightarrow 0$, such that we expect the vortices to vanish and the current to be unaffected by the magnetic field, regardless of the magnetic field strength.

We use γ (5.33) in equation (5.12) and (5.3) to calculate the current density numerically and the result is shown in figure 5.4 for three different wavelengths. The distance between the vortices is changed when the wavelength of the magnetic field is changed, as we predicted analytically. And for some wavelengths, e.g. $\lambda = L/2$, the vortices vanish completely.

The total current is found in the same manner as in section 5.3.1, giving

$$I_x = I_{c,0} \sin \Delta \varphi \frac{\sin(\frac{e}{\hbar} \Phi)}{\frac{e}{\hbar} \Phi} \quad (5.35)$$

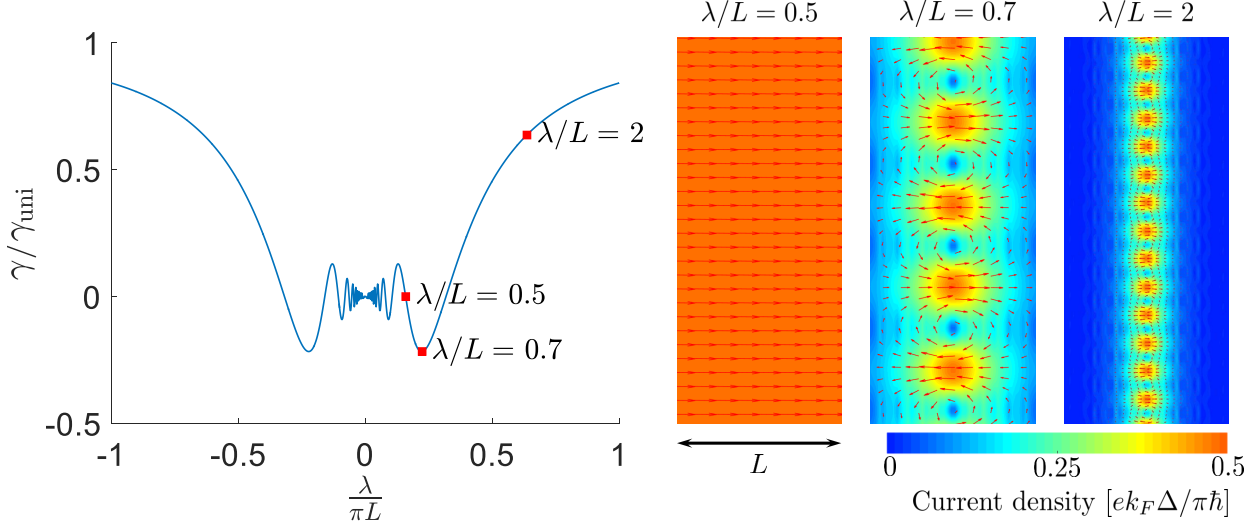


Figure 5.4: The left plot shows the phase shift γ , relative to the phase shift, γ_{uni} , in a uniform field, versus the wavelength λ of an applied sinusoidal magnetic field varying along the Josephson junction. The scale plots shows the current density in the junction for three different wavelengths λ , all for the same magnetic field strength $l_m/L = 0.3$. The wavelength of each scale plot is indicated in the γ -plot. When $\lambda = 0.5L$ the phase shift is $\gamma = 0$ and the current density is uniform. The γ -plot is calculated from equation (5.33) and the scale plots are calculated from equation (5.3), (5.12) and (5.33) at temperature $k_B T = \Delta$.

where Φ is the magnetic flux:

$$\Phi = \int \mathbf{B} \cdot d\mathbf{A} = \Phi_{\text{uni}} \frac{\sin(\pi L/\lambda)}{\pi L/\lambda}, \quad (5.36)$$

with $\Phi_{\text{uni}} = BWL$ as the magnetic flux in the uniform field. In terms of magnetic flux this expression is identical to the total current in the uniform field. However, the flux, and consequently the total and critical current, will be dependent on the wavelength. The high temperature critical current will be given as

$$I_c = I_{c,0} \left| \frac{\sin\left(\frac{LW}{l_m^2} \frac{\sin(\pi L/\lambda)}{\pi L/\lambda}\right)}{\frac{LW}{l_m^2} \frac{\sin(\pi L/\lambda)}{\pi L/\lambda}} \right|. \quad (5.37)$$

We find the period of the Fraunhofer oscillations to be given as $d_{\text{vortex}}\Phi_{\text{uni}}/W$ with $\Phi_{\text{uni}} = BLW$, so that the Fraunhofer oscillations are related to the vortex pattern in the same manner as the uniform field. In figure 5.5 the critical current obtained from numerical computation is shown for different wavelengths, λ , and varying magnetic field strength, B . We recognize the Fraunhofer pattern as we had for the uniform field, but the decay can be controlled by changing the wavelength, λ , and for some wavelengths, e.g. $\lambda = L/2$, the critical current maintains constant regardless of the field strength. We propose that this can be understood as an interference phe-

nomenon where the phase-shift picked up by the electrons and holes comprising the ABS level are completely cancelled out due to the specific magnetic field profile. The fact that the supercurrent survives for arbitrarily large field strengths, B , as long as the spacial modulation wavelengths satisfy $\lambda = L/n$ is remarkable and is one of the key findings in this thesis.

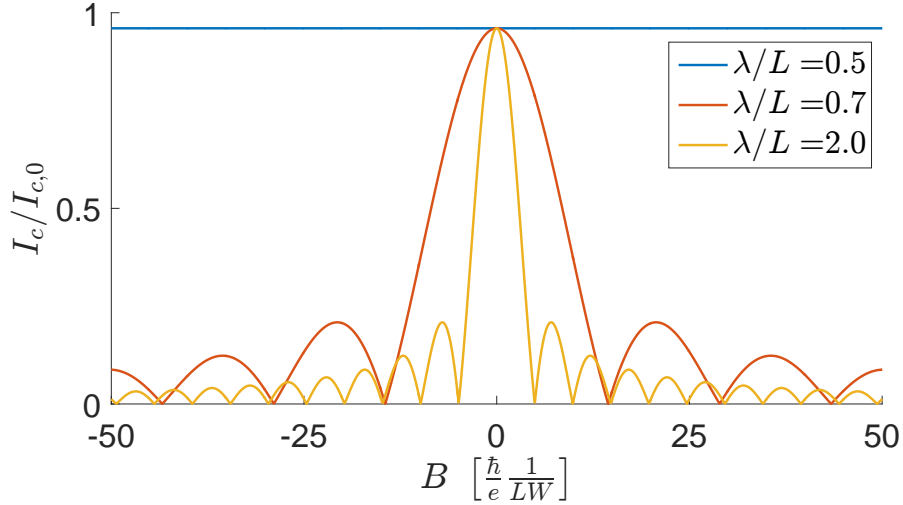


Figure 5.5: Plot of the critical current I_c versus the magnetic field strength B in a symmetric periodic field varying with three wavelengths, λ , along the junction in the normal region. The current is calculated numerically from equation (5.1), (5.12) and (5.33) at $\Delta\varphi = \pi/2$.

Anti-symmetric field

Taking φ to zero in (5.30) the magnetic field becomes anti-symmetric about the y -axis, and the first term in (5.32) vanishes:

$$\gamma = \frac{L^2}{l_m^2} \tan \theta_k \left[\left(\frac{\lambda}{\pi L} \right)^2 \sin \left(\frac{\pi L}{\lambda} \right) - \frac{\lambda}{\pi L} \cos \left(\frac{\pi L}{\lambda} \right) \right]. \quad (5.38)$$

We notice how γ now is position-independent and expect a uniform current distribution without current vortices. The magnetic wavelength dependency of γ is shown in figure 5.6(a). For certain wavelengths, λ , γ will be zero regardless of the field strength or position and we expect the current to be unaffected by the magnetic field. Using the expression for γ (5.38) in equation (5.12) and (5.3) the current density is found numerically and the result is shown in figure 5.6(b) for varying wavelengths, λ , of the external field.

We find the total current in the high temperature regime as we did for the uniform field in sec-

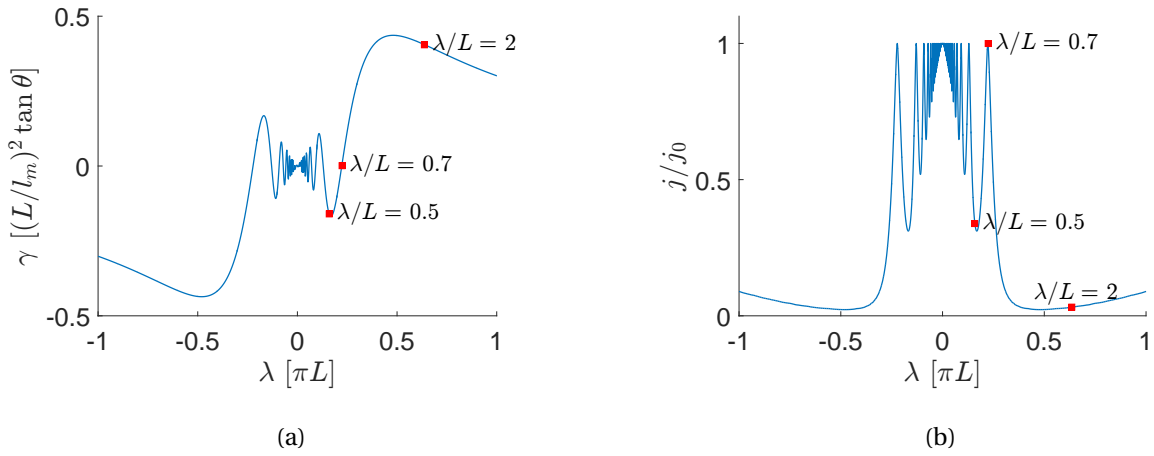


Figure 5.6: Plot of the phase shift γ (a) and the uniform current density (b) versus the wavelength of an anti-symmetric applied magnetic field varying periodically along the junction. The γ -plot is calculated from equation (5.38) and the current density is calculated from equation (5.3), (5.12) and (5.38) at temperature $k_B T = \Delta$ and magnetic length $l_m/L = 0.3$. Three wavelengths ($\lambda/L = 0.5$, $\lambda/L = 0.7$ and $\lambda/L = 2$) are marked in each plot for comparison with figure 5.7.

tion 5.3.1. As γ (5.32) is independent of y_0 , equation (5.24) yields

$$I = \frac{I_{c,0}}{2} \int_{-\pi/2}^{\pi/2} d\theta_k \cos \theta_k \sin(\Delta\varphi - \gamma). \quad (5.39)$$

Using that $\gamma(\theta_k) = -\gamma(-\theta_k)$ this can be rewritten to

$$I = I_{c,0} \sin \Delta\varphi \int_0^{\pi/2} d\theta_k \cos \theta_k \cos \gamma. \quad (5.40)$$

After inserting for γ and integrating over θ_k we obtain the total current,

$$I = I_{c,0} \sin \Delta \varphi \frac{L^2}{l_m^2} |f(\lambda)| K_1 \left(\frac{L^2}{l_m^2} |f(\lambda)| \right), \quad (5.41)$$

where $K_1(z)$ is the modified Bessel function of second kind and we have defined

$$f(\lambda) \equiv \left(\frac{\lambda}{\pi L} \right)^2 \sin \left(\frac{\pi L}{\lambda} \right) - \frac{\lambda}{\pi L} \cos \left(\frac{\pi L}{\lambda} \right). \quad (5.42)$$

Hence, the high temperature critical current is

$$I_c = I_{c,0} \frac{L^2}{l_m^2} |f(\lambda)| K_1\left(\frac{L^2}{l_m^2} |f(\lambda)|\right). \quad (5.43)$$

The wavelengths λ that make $f(\lambda)$ go to zero, will give $I_c = I_{c,0}$, regardless of the magnetic field strength. In figure 5.7 the critical current obtained from numerical computation is shown for different wavelengths, λ , and varying magnetic field strength, B . This result is in correspondance with the analytical expression (5.43). We notice that we no longer have the familiar Fraunhofer pattern and understand this as being a consequence of the absence of the current vortices. Just like we found for the symmetric field there exists wavelengths, e.g. $\lambda \approx 0.7L$, which make the critical current I_c remain constant when the magnetic field strength increases.

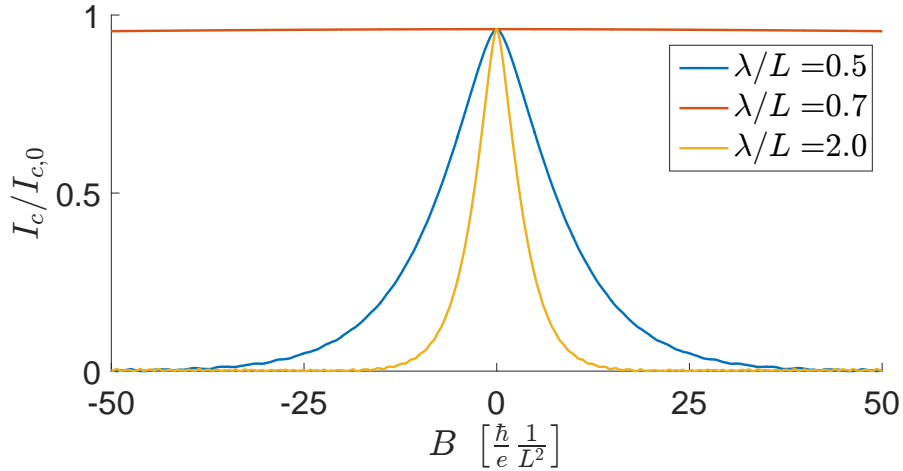


Figure 5.7: Plot of the critical current I_c versus the magnetic field strength B in a anti-symmetric periodic field varying with three wavelengths, λ , along the junction in the normal region. The current is calculated numerically from equation (5.1), (5.12) and (5.38) at $\Delta\varphi = \pi/2$.

5.3.3 Sinusoidal field varying along the interfaces

Instead of varying the field along the junction we will now consider a sinusoidal magnetic field varying along the interfaces:

$$\mathbf{B} = B \sin\left(\frac{2\pi}{\lambda} y + \varphi\right) [\Theta(x + L/2) - \Theta(x - L/2)] \hat{z} \quad (5.44)$$

with the gauge

$$\mathbf{A} = B \frac{\lambda}{2\pi} \cos\left(\frac{2\pi}{\lambda} y + \varphi\right) [\Theta(x + L/2) - \Theta(x - L/2)] \hat{x}. \quad (5.45)$$

Now the phase shift is

$$\gamma = -\frac{\lambda L}{l_m^2 \pi} \frac{\sin\left(\frac{\pi L}{\lambda} \tan \theta_k\right)}{\frac{\pi L}{\lambda} \tan \theta_k} \cos\left(\frac{2\pi}{\lambda} [y_0 - x_0 \tan \theta_k] + \varphi\right). \quad (5.46)$$

As we did in the previous section we will also here look at the symmetric- and anti-symmetric fields taking φ to $\pi/2$ and 0, respectively.

Symmetric field

In the symmetric field, i.e. when $\varphi = \pi/2$, the phase shift is

$$\gamma = \frac{\lambda L}{l_m^2 \pi} \frac{\sin\left(\frac{\pi L}{\lambda} \tan \theta_k\right)}{\frac{\pi L}{\lambda} \tan \theta_k} \sin\left(\frac{2\pi}{\lambda} [y_0 - x_0 \tan \theta_k]\right). \quad (5.47)$$

In the limit with $\lambda \gg L$ and $\lambda \gg y_0$ the phase shift will approach the phase shift in the uniform field, $\gamma \rightarrow \gamma_{\text{uni}}$:

$$\gamma \rightarrow \frac{\lambda L}{l_m^2 \pi} \left(\frac{2\pi}{\lambda} [y_0 - x_0 \tan \theta_k] \right) = \frac{2L}{l_m^2} (y_0 - x_0 \tan \theta_k) \quad (5.48)$$

where we have used that $\sin(x) \approx x$ when $x \ll 1$. This is as expected as a symmetric periodical function will be approximately uniform when the wavelength becomes very large. In the limit with $\lambda \ll L$ the sinc-function in the second factor in (5.47) will go to zero and the effect of the magnetic field on the current will vanish.

The vortex distance will for this field vary periodically along the y -axis. As we did for the uniform field we find the vortex distance, d_{vortex} , from the relation

$$\gamma(y_0 + d_{\text{vortex}}) = \gamma(y_0) + 2\pi. \quad (5.49)$$

Inserting for γ (5.47) and solving for d_{vortex} gives

$$d_{\text{vortex}} = x_0 \tan \theta_k - y_0 + \frac{\lambda}{2\pi} \arcsin \left[\sin\left(\frac{2\pi}{\lambda} [y_0 - x_0 \tan \theta_k]\right) + 2 \frac{l_m^2 \pi^2}{\lambda L} \frac{\frac{\pi L}{\lambda} \tan \theta_k}{\sin\left(\frac{\pi L}{\lambda} \tan \theta_k\right)} \right] - n\lambda. \quad (5.50)$$

where n in the last term is any integer which we soon will put to zero in order to obtain the distance between the closest neighboring vortices. This is a rather complicated expression depending on both x_0 , y_0 and θ_k , and we expect this new dependency to modify the vortex pattern. In the limit of $\lambda \gg L$ and $\lambda \gg y_0$ the expression in (5.50) approaches the vortex distance in the

uniform field:

$$\begin{aligned}
 d_{\text{vortex}} &\rightarrow x_0 \tan \theta_k - y_0 + \frac{\lambda}{2\pi} \arcsin \left(\frac{2\pi}{\lambda} \left[y_0 - x_0 \tan \theta_k + \frac{l_m^2 \pi}{L} \right] \right) - n\lambda \\
 &\rightarrow x_0 \tan \theta_k - y_0 + y_0 - x_0 \tan \theta_k + \pi \frac{l_m^2}{L} - n\lambda \\
 &= \pi \frac{l_m^2}{L}
 \end{aligned} \tag{5.51}$$

where we in the last equality has taken n to be zero in order to get the distance between the neighboring vortices. This is the vortex distance we found for the uniform field (5.19) and corresponds to the limit found in equation (5.48). We stated above that vortex distance would vary periodically along the y -axis. This means that there is a distance, d_{chain} , which satisfy

$$d_{\text{vortex}}(y_0 + d_{\text{chain}}) = d_{\text{vortex}}(y_0) + m d_{\text{chain}}, \tag{5.52}$$

with m as an integer. From eqaution (5.50) we find that this is satisfied if we let $m = 1$ and $d_{\text{chain}} = \lambda$. Thus we expect the pattern to be *chains* of vortices separated by a x_0 and y_0 dependent distance d_{vortex} and with each chain center separated by λ . Moreover, just like the vortices, the chains will also appear as chains and anti-chains, with the distance between neighboring chains and anti-chains $d_{\text{chain}} = \lambda/2$. This can be seen from equation (5.47) in which we notice that $\gamma(y_0 + \lambda/2) = -\gamma(y_0)$. We will consider the center of a chain as the point where d_{vortex} is sortest, i.e. where the vortex density is largest. By setting x_0 and θ_k to zero in equation (5.50) we find d_{vortex} to be shortest at $y_0 = n\lambda$ and setting $n = 0$ we expect the first chain to be placed with it's center at $y_0 = 0$.

Unlike we saw in the uniform field, the vortex pattern for the field considered here depend on the superconducting phase difference, $\Delta\varphi$. We check the dependency $\Delta\varphi$ has on the current density in the same manner as we did for the uniform field, namely considering equation (5.12) in which we see that a phase difference $\delta\varphi$ in the superconducting phase corresponds to a phase shift $-\delta\varphi$ in γ . In the uniform field we found that such phase shift only gave a shift along the interface, $\gamma_{\text{uni}}(y_0) - \delta\varphi = \gamma_{\text{uni}}(y_0 - \delta\varphi l_m^2 / 2L)$, and did not change the pattern. In the field considered in this section this relation does not apply and we expect the superconducting phase difference to affect the pattern. More specifically we can consider the relation between the chains and anti-chains. If we take $\Delta\varphi = 0$ we find from equation (??) that a shift $d_{\text{chain}}/2 = \lambda/2$ which would take us from a chain to an anti-chain (or the other way around) will give

$$\delta I(y_0 + \lambda/2) = \frac{I_{c,0}}{k_F W} \sin(\gamma(y_0 + \lambda/2)) = -\frac{I_{c,0}}{k_F W} \sin(\gamma) = -\delta I(y_0) \tag{5.53}$$

and the current in the anti-chain is in fact opposite of the current in the chain. However, if we take the superconducting phase difference to be $\Delta\varphi = \pi/2$, the current density becomes symmetrically dependent on γ :

$$\delta I(y_0 + \lambda/2) = \frac{I_{c,0}}{k_F W} \cos(\gamma(y_0 + \lambda/2)) = \frac{I_{c,0}}{k_F W} \cos(\gamma) = \delta I(y_0) \quad (5.54)$$

such that the current in the anti-chains and the chains are identical. The vortex pattern can in this case be thought of as a linear arrangement of chains centers separated by a distance $d_{\text{chain}} = \lambda/2$, in contrast to the chain- anti-chain arrangement we get if the the superconducting phase difference is zero.

The current density was found numerically from equation (5.12) and (5.3) and the result is shown in figure 5.8 for different wavelengths. We observe what was predicted, namely a repeated pattern of vortex-anti-vortex-chains along the interfaces. With $\Delta\varphi = 0$ we observe a chain- anti-chain pattern with each chain separated by $d_{\text{chain}} = \lambda$. With $\Delta\varphi = \pi/2$ there are no anti-chains as the current density is an even function of γ and each chain is separated by $\lambda/2$. Moreover, the current density approaches a uniform distribution as $\lambda \rightarrow 0$ with current as given in equation (5.7), as we predicted analytically. When $\lambda \gg L$ the uniform field pattern reappears, as predicted. As the expression for γ is quite complicated we can not calculate the total current analytically, even in the high temperature regime. However, the critical current is found numerically and the result is shown in figure 5.9. For large wavelengths, λ , the critical current approaches the Fraunhofer pattern as we would expect from the pattern we found in the current density. The critical current smoothens out and approaches the constant critical current $I_{c,0}$ when the wavelength goes to zero, in correspondence with the limit found above !!!REFEQ!!!.

Anti-symmetric field

We now let $\varphi = 0$ in equation (??) such that the magnetic field is anti-symmetric about the x -axis with the phase shift

$$\gamma = -\frac{L^2}{l_m^2 \pi L} \frac{\lambda}{\pi L} \frac{\sin(\frac{\pi L}{\lambda} \tan \theta_k)}{\frac{\pi L}{\lambda} \tan \theta_k} \sin\left(\frac{2\pi}{\lambda} \left[\left(y_0 + \frac{\lambda}{4}\right) - x_0 \tan \theta_k\right]\right) \quad (5.55)$$

This is equal to the symmetric field (5.47), only shifted by $\lambda/4$ along the y -axis. More general a phase φ in (??) give a pattern like we found for the symmetric field, only shifted by $\frac{\lambda}{2\pi} (\frac{\pi}{2} - \varphi)$ along the interface. Hence we expect a similar, but shifted pattern as for the symmetric field. With $\varphi = 0$ the first chain will be centered at $\lambda/4$ with a corresponding anti-chain centered at

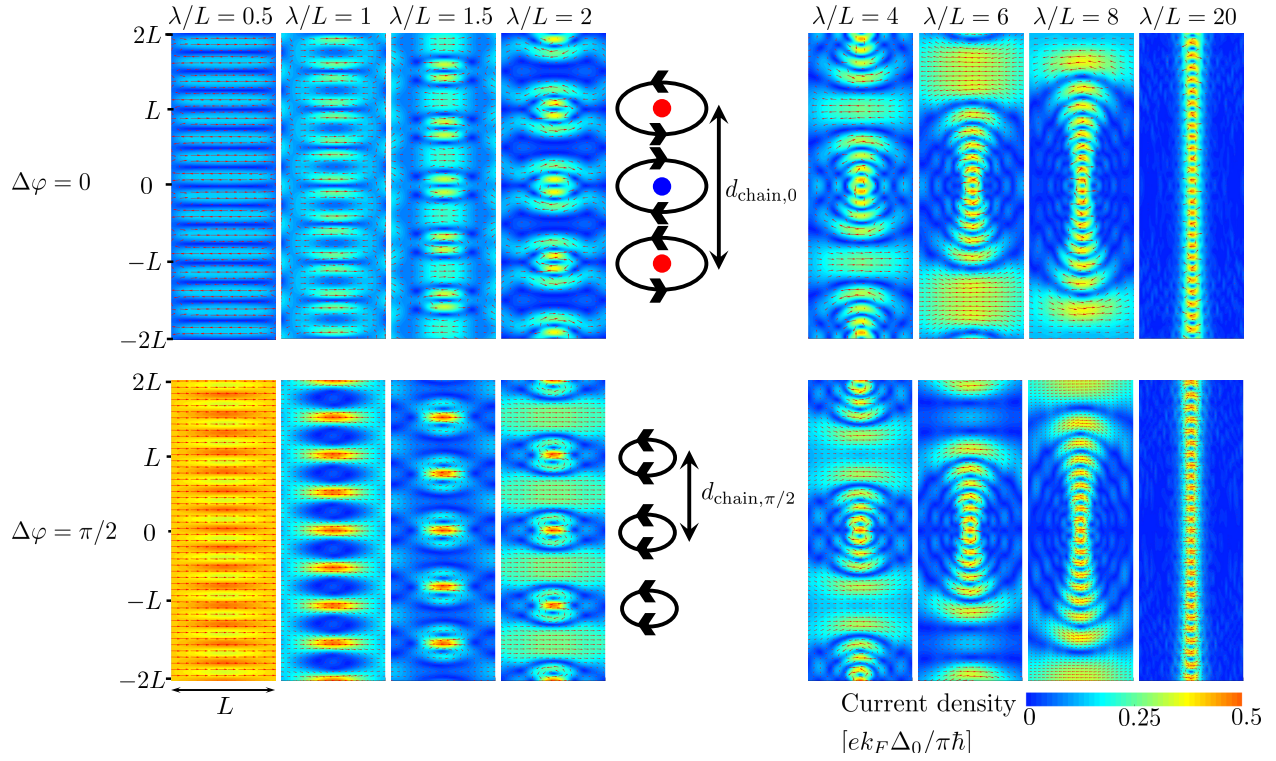


Figure 5.8: Scale plots of the supercurrent density in a magnetic field varying periodically with wavelength λ along the superconducting region. The eight plot in the upper and lower row show the current density when the superconducting phase difference, $\Delta\varphi$, is zero and $\pi/2$, respectively. Chains (red) and anti-chains (blue) are indicated for the scale plot of wavelength $\lambda/L = 2$, along with the chain distance d_{chain} . When $\Delta\varphi = \pi/2$ the chains and anti-chains are identical such that the chain distance is halved, $d_{\text{chain},0} = 2d_{\text{chain},\pi/2}$. The current densities are calculated from equation (5.3), (5.12) and (5.47) at temperature $k_B T = \Delta$ and magnetic length $l_m/L = 0.3$.

$-\lambda/4$. In fact for every chain centered at y_0 we expect to find an anti-chain centered at $-y_0$. Hence, the anti-symmetric field generate an anti-symmetric pattern about the x -axis, unlike the symmetric field in which a chain centered at y_0 imply an identical chain centered at $-y_0$. Of course if the superconducting phase difference is $\Delta\varphi = 2\pi$, such that the current density is an even function of γ , the anti-chains turn into chains and also the anti-symmetric field reveals a symmetric pattern. This current density found from numerical calculations are shown in figure (5.10).

Since the current density of the symmetric and anti-symmetric field along the interface only differ by a shift of the center of the vortex rows along the y -axis, we expect the total current to be equal in the two cases, when $W \gg L$. This has also been confirmed numerically, and the critical current in the anti-symmetric field (or for any field of the form given in equation (??) for that matter) will be as shown in figure 5.9.

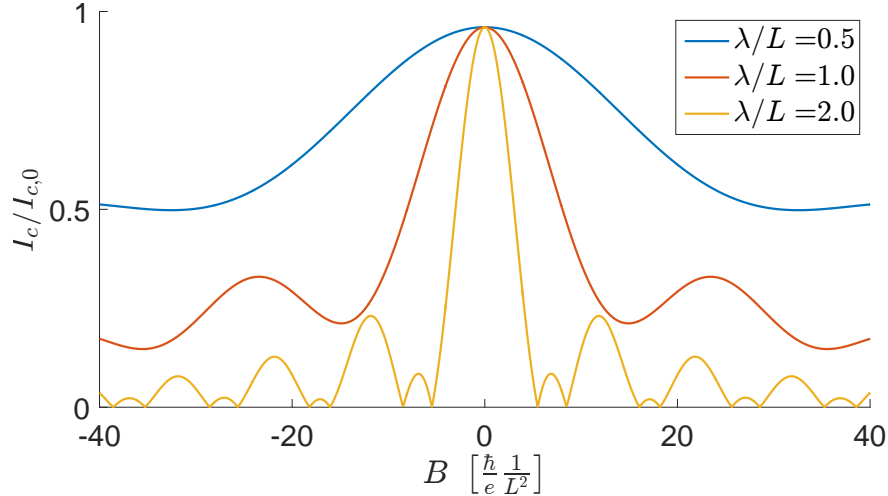


Figure 5.9: Plot of the critical current I_c versus the magnetic field strength B in a periodic field varying with three wavelengths, λ , along the superconducting interface in the normal region. The current is calculated numerically from equation (5.1), (5.12) and (5.47) at $\Delta\varphi = \pi/2$.

We have in this section found that with a field of the form in equation (??), varying periodically along the interface, we are able to control the pattern by changing the wavelength λ and the phase φ , as well as the superconducting phase difference $\Delta\varphi$ and the magnetic field strength B . This is a possibility we did not have in the uniform field in which we could control the vortex distance and size but not the shape of the pattern. The fact that we can control in which areas of the junction the current is dominant give rise to many new possibilities. Such as

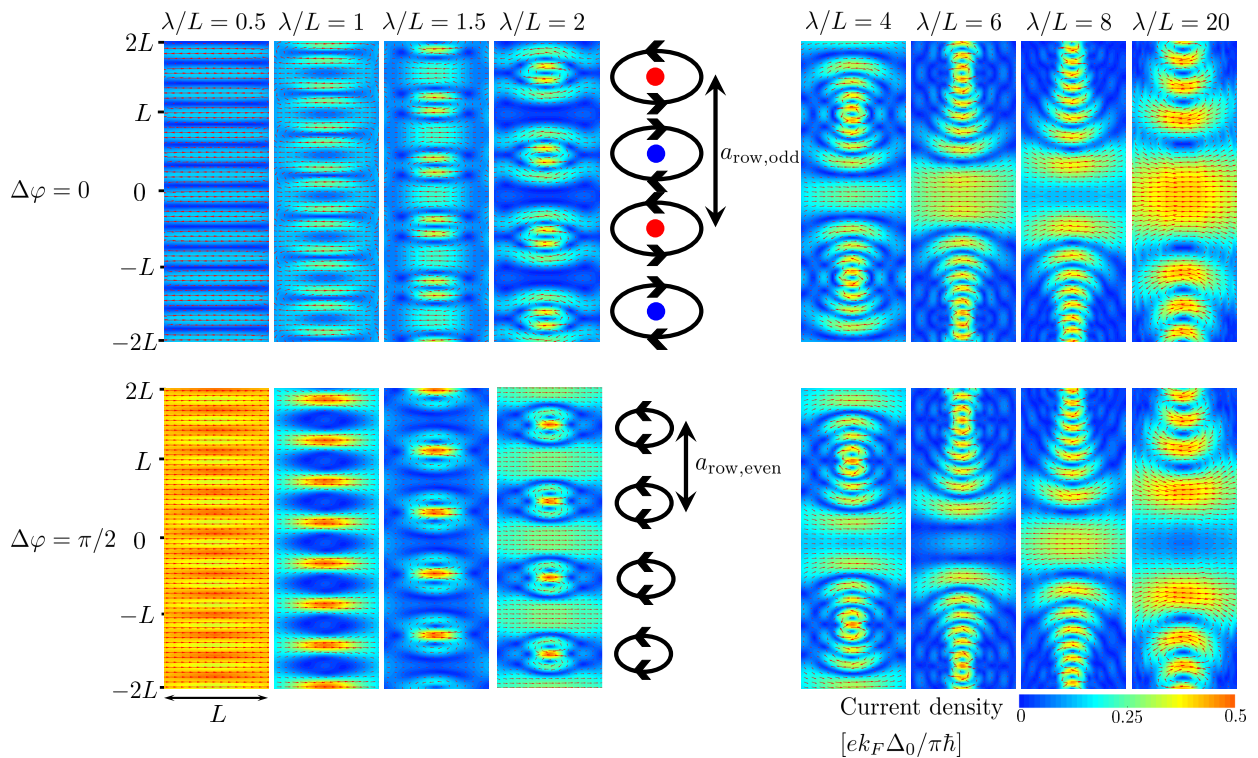


Figure 5.10: blabla.. Planen her å gjøre figurene litt finere sånn som for konstant felt. Og vise to rader med bilder, en med $\Delta\varphi = 0$ og en med $\Delta\varphi = \pi/2$

Chapter 6

Conclusion and outlook

In this thesis we have studied how the supercurrent density and the critical current in a SNS-junction is affected by an external magnetic field. The result found from a uniform magnetic field is already known [7, 8], however we have here considered modulated magnetic fields and seen how we are able to control the supercurrent via the magnetic field. A key observation is that the supercurrent will be unaffected by the magnetic field for some modulations regardless of the field strength.

In chapter 4 we found the energy levels of the Andreev bound states which we in chapter 5 used to find the current density and critical current. We showed how the magnetic field accumulate a phase shift γ in the superconducting phase which depend on the field modulation and strength, as well as the trajectory of the electrons and holes, and thus give rise to quantum interference of the supercurrent. The modulations considered was a uniform field, a sinusoidal field varying along the junction and a sinusoidal field varying along the interfaces.

In the uniform field a row of Josephson vortices appeared in the center of the junction along the interface and the critical current was found to be the familiar Fraunhofer oscillations, in accordance with earlier research [17–21, 25]. We found the same kind of vortex row in the symmetric sinusodial field varying along the junction. However, now the distance between the vortices could be controlled by changing the wavelength of the magnetic field and for some wavelengths we even found the current to be unaffected by the field. In the anti-symmetric field varying along the junction the Josephson vortices and Fraunhofer oscillations disappeared leaving a uniform current density. The wavelength of the magnetic field could be used to control the magnitude of the current and like the symmetric field some wavelengths left the supercurrent unaffected by the field. In the field varying along the interface the vortex row that was observed in the uniform field was repeated as rows and anti-rows in the center of the junction along the interfaces.

Unlike the uniform field, we then found the current density pattern to depend on the superconducting phase difference, $\Delta\varphi$.

The analysis did in this thesis is based on several simplifications, such as transparent barriers at the superconducting interfaces and negligence of the Lorentz effect on the trajectories of the electrons and holes. In future work we may consider a more realizable system where we take into account barriers and the Lorentz force, as well as the modulated magnetic field, and in such analysis we expect the method considered in section 5.2 to be useful. Moreover, we have here only considered a circular Fermi surface. In a uniform field with warped Fermi surface, earlier research has shown the appearance of a 2D-pattern of Josephson vortices, unlike the single vortex chain we have seen here [25]. It would be interesting to also consider how non-uniform modulations of the magnetic field would affect the current for such Fermi surfaces. In this thesis we considered the effect originating from the vector potential of the magnetic field. However, the magnetic field will also effect the spin properties of the electrons and holes via the Zeeman-effect !!!CITE!!!. It is reasonable to neglect the Zeeman-effect for the SNS-junction considered in this thesis as the effect from the vector potential will be much more dominant !!!CITE!!!. However, if one replace the normal metal in the SNS-junction with a ferromagnet (SFS), the Zeeman-effect will be much more prominent !!!CITE!!!, and it would be interesting to study how this affects the current in the junction. Lastly, we have here considered s-wave superconductors with isotropic superconducting gap !!!CITE!!!, and it would be interesting to instead consider the effect of magnetic field on a junction consisting of anisotropic d-wave superconductors, which to our knowledge has still not been explored.

Appendix A

Additional Information

A.1 Commutation relations

$$[c_{\mathbf{k},\sigma}^\dagger, c_{\mathbf{k}',\sigma'}]_+ = \delta_{\mathbf{k},\mathbf{k}'} \delta_{\sigma,\sigma'} \quad (\text{A.1a})$$

$$[c_{\mathbf{k},\sigma}^\dagger, c_{\mathbf{k}',\sigma'}^\dagger]_+ = 0 \quad (\text{A.1b})$$

$$[c_{\mathbf{k},\sigma}, c_{\mathbf{k}',\sigma'}]_+ = 0 \quad (\text{A.1c})$$

A.2 The pauli matrices

$$\sigma \quad (\text{A.2})$$

Bibliography

- [1] Dirk van Delft and Peter Kes. The discovery of superconductivity. 63(9):38–43, September 2010. ISSN 0031-9228, 1945-0699. URL <http://physicstoday.scitation.org/doi/full/10.1063/1.3490499>.
- [2] W. Meissner and R. Ochsenfeld. Ein neuer effekt bei eintritt der supraleitfähigkeit. *Naturwissenschaften*, 21(44):787–788, 1933. ISSN 1432-1904. URL <http://dx.doi.org/10.1007/BF01504252>.
- [3] J. Bardeen, L. N. Cooper, and J. R. Schrieffer. Theory of superconductivity. *Phys. Rev.*, 108: 1175–1204, December 1957. URL <http://link.aps.org/doi/10.1103/PhysRev.108.1175>.
- [4] R. D. Parks. *Superconductivity*. CRC Press, 1969. ISBN 978-0-8247-1521-2. URL <https://books.google.com/books?id=D4hK-yGBEmoC&pg=PA1005>.
- [5] B. Pannetier and H. Courtois. Andreev reflection and proximity effect. *Journal of Low Temperature Physics*, 118(5):599–615, 2000. ISSN 1573-7357. URL <http://dx.doi.org/10.1023/A:1004635226825>.
- [6] JM Rowell. Magnetic field dependence of the josephson tunnel current. *Physical Review Letters*, 11(5):200, 1963. URL <http://journals.aps.org/prl/abstract/10.1103/PhysRevLett.11.200>.
- [7] Michael Tinkham. *Introduction to Superconductivity*. Courier Corporation, 1996. ISBN 978-0-486-13472-7.
- [8] Antonio Barone and Gianfranco Paternò. *Physics and applications of the Josephson effect*. Wiley, 1982. ISBN 978-0-471-01469-0.
- [9] Jarillo-Herrero P. Oostinga J. B. Vandersypen L. M. K. Heersche, H. B. and A. F. Morpurgo. Bipolar supercurrent in graphene. *Nature*, 446.

- [10] CaladoV. E., GoswamiS., NandaG., DiezM., AkhmerovA. R., WatanabeK., TaniguchiT., KlapwijkT. M., and VandersypenL. M. K. Ballistic Josephson junctions in edge-contacted graphene. *Nat Nano*, 10(9):761–764, September 2015. ISSN 1748-3387. URL <http://dx.doi.org/10.1038/nano.2015.156>.
- [11] M. T. Allen, O. Shtanko, I. C. Fulga, J. I. J. Wang, D. Nurgaliev, K. Watanabe, T. Taniguchi, A. R. Akhmerov, P. Jarillo-Herrero, L. S. Levitov, and A. Yacoby. Visualization of phase-coherent electron interference in a ballistic graphene josephson junction, 2015.
- [12] Zhu-M. J. Fal’ko V. I. Mishchenko A. Kretinin A. V. Novoselov K. S. Woods C. R. Watanabe K. Taniguchi T. Geim A. K. Ben Shalom, M. and J. R. Prance. Quantum oscillations of the critical current and high-field superconducting proximity in ballistic graphene. *Nat Phys*, 12(4):318–322, April 2016. ISSN 1745-2473. URL <http://dx.doi.org/10.1038/nphys3592>.
- [13] M. Veldhorst, M. Snelder, M. Hoek, T. Gang, V. K. Guduru, X. L. Wang, U. Zeitler, W. G. van der Wiel, A. A. Golubov, H. Hilgenkamp, and A. Brinkman. Josephson supercurrent through a topological insulator surface state. *Nat Mater*, 11(5):417–421, May 2012. ISSN 1476-1122. doi: 10.1038/nmat3255. URL <http://dx.doi.org/10.1038/nmat3255>.
- [14] J. R. Williams, A. J. Bestwick, P. Gallagher, Seung Sae Hong, Y. Cui, Andrew S. Bleich, J. G. Analytis, I. R. Fisher, and D. Goldhaber-Gordon. Unconventional josephson effect in hybrid superconductor-topological insulator devices. *Phys. Rev. Lett.*, 109:056803, Jul 2012. doi: 10.1103/PhysRevLett.109.056803. URL <http://link.aps.org/doi/10.1103/PhysRevLett.109.056803>.
- [15] Sean Hart, Hechen Ren, Timo Wagner, Philipp Leubner, Mathias Muhlbauer, Christoph Brune, Hartmut Buhmann, Laurens W. Molenkamp, and Amir Yacoby. Induced superconductivity in the quantum spin Hall edge. *Nat Phys*, 10(9):638–643, September 2014. ISSN 1745-2473. URL <http://dx.doi.org/10.1038/nphys3036>.
- [16] Vlad S. Pribiag, BeukmanArjan J. A., Fanming Qu, Maja C. Cassidy, Christophe Charpentier, Werner Wegscheider, and Leo P. Kouwenhoven. Edge-mode superconductivity in a two-dimensional topological insulator. *Nat Nano*, 10(7):593–597, July 2015. ISSN 1748-3387. URL <http://dx.doi.org/10.1038/nano.2015.86>.
- [17] J. C. Cuevas and F. S. Bergeret. Magnetic interference patterns and vortices in diffusive sns junctions. 2007. doi: 10.1103/PhysRevLett.99.217002.
- [18] F. S. Bergeret and J. C. Cuevas. The Vortex State and Josephson Critical Current of a Diffusive SNS Junction. *Journal of Low Temperature Physics*, 153(5):304–324, 2008.

- ISSN 1573-7357. doi: 10.1007/s10909-008-9826-2. URL <http://dx.doi.org/10.1007/s10909-008-9826-2>.
- [19] Mohammad Alidoust, Granville Sewell, and Jacob Linder. Non-fraunhofer interference pattern in inhomogeneous ferromagnetic josephson junctions. *Phys. Rev. Lett.*, 108:037001, Jan 2012. doi: 10.1103/PhysRevLett.108.037001. URL <http://link.aps.org/doi/10.1103/PhysRevLett.108.037001>.
- [20] Mohammad Alidoust and Klaus Halterman. Proximity induced vortices and long-range triplet supercurrents in ferromagnetic josephson junctions and spin valves. 2015. doi: 10.1063/1.4908287.
- [21] Morten Amundsen and Jacob Linder. General solution of 2d and 3d superconducting quasiclassical systems: coalescing vortices and nanoisland geometries. 2015.
- [22] J. P. Heida, B. J. van Wees, T. M. Klapwijk, and G. Borghs. Nonlocal supercurrent in mesoscopic josephson junctions. *Phys. Rev. B*, 57:R5618–R5621, Mar 1998. doi: 10.1103/PhysRevB.57.R5618. URL <http://link.aps.org/doi/10.1103/PhysRevB.57.R5618>.
- [23] Victor Barzykin and Alexandre M. Zagoskin. Coherent transport and nonlocality in mesoscopic SNS junctions: anomalous magnetic interference patterns. *Superlattices and Microstructures*, 25(5):797 – 807, 1999. ISSN 0749-6036. doi: <http://dx.doi.org/10.1006/spmi.1999.0731>. URL <http://www.sciencedirect.com/science/article/pii/S0749603699907310>.
- [24] Minsoo Kim, Dongchan Jeong, Gil-Ho Lee, Yun-Sok Shin, Hyun-Woo Lee, and Hu-Jong Lee. Tuning Locality of Pair Coherence in Graphene-based Andreev Interferometers. *Scientific Reports*, 5:8715, March 2015. URL <http://dx.doi.org/10.1038/srep08715>.
- [25] V. P. Ostroukh, B. Baxevanis, A. R. Akhmerov, and C. W. J. Beenakker. Two-dimensional josephson vortex lattice and anomalously slow decay of the fraunhofer oscillations in a ballistic sns junction with a warped fermi surface. *Phys. Rev. B*, 94:094514, Sep 2016. doi: 10.1103/PhysRevB.94.094514. URL <http://link.aps.org/doi/10.1103/PhysRevB.94.094514>.
- [26] Hendrik Meier, Vladimir I. Fal'ko, and Leonid I. Glazman. Edge effects in the magnetic interference pattern of a ballistic sns junction. *Phys. Rev. B*, 93:184506, May 2016. doi: 10.1103/PhysRevB.93.184506. URL <http://link.aps.org/doi/10.1103/PhysRevB.93.184506>.

- [27] A M Forrest. Meissner and ochsenfeld revisited. *European Journal of Physics*, 4(2):117, 1983.
URL <http://stacks.iop.org/0143-0807/4/i=2/a=011>.
- [28] F. London and H. London. The electromagnetic equations of the supraconductor. *Proceedings of the Royal Society of London A: Mathematical, Physical and Engineering Sciences*, 149 (866):71–88, 1935. ISSN 0080-4630. URL <http://rspa.royalsocietypublishing.org/content/149/866/71>.
- [29] P. G. de Gennes. Boundary effects in superconductors. *Rev. Mod. Phys.*, 36:225–237, Jan 1964. URL <http://link.aps.org/doi/10.1103/RevModPhys.36.225>.
- [30] A. F. Andreev. The thermal conductivity of the intermediate state in superconductors. *Sov. Phys. JETP*, 19:1228 – 1231, Nov 1964. URL <http://www.jetp.ac.ru/cgi-bin/e/index/e/19/5/p1228?a=list>.
- [31] G. E. Blonder, M. Tinkham, and T. M. Klapwijk. Transition from metallic to tunneling regimes in superconducting microconstrictions: Excess current, charge imbalance, and supercurrent conversion. *Phys. Rev. B*, 25:4515–4532, Apr 1982. URL <http://link.aps.org/doi/10.1103/PhysRevB.25.4515>.
- [32] B. D. Josephson. Possible new effects in superconductive tunnelling. *Physics Letters*, 1 (7):251 – 253, 1962. ISSN 0031-9163. URL <http://www.sciencedirect.com/science/article/pii/0031916362913690>.